Towards an Effective Spin Hamiltonian of the Pyrochlore Spin Liquid $Tb_2Ti_2O_7$

Hamid R. Molavian,[1] Paul A. McClarty,[1] and Michel J. P. Gingras[1,2]

[1] *Department of Physics and Astronomy, University of Waterloo, Waterloo, ON, N2L 3G1, Canada.*
[2] *Canadian Institute for Advanced Research, 180 Dundas Street West, Suite 1400, Toronto, ON, M5G 1Z8, Canada.*

(Dated: December 15, 2009)

$Tb_2Ti_2O_7$ is a pyrochlore antiferromagnet that has dynamical spins and only short-range correlations even at 50 mK − the lowest temperature explored so far − which is much smaller than the scale set by the Curie-Weiss temperature $\theta_{\rm CW} \approx -14$ K. The absence of long-range order in this material is not understood. Recently, virtual crystal field excitations (VCFEs) have been shown to be significant in $Tb_2Ti_2O_7$, but their effect on spin correlations has not been fully explored. Building on the work in Phys. Rev. Lett. **98**, 157204 (2007), we present details of an effective Hamiltonian that takes into account VCFEs. Previous work found that VCFEs-induced renormalization of the nearest neighbor Ising exchange leads to spin ice correlations on a single tetrahedron. In this paper, we construct an effective spin-1/2 low-energy theory for $Tb_2Ti_2O_7$ on the pyrochlore lattice. We determine semiclassical ground states on a lattice that allow us to see how the physics of spin ice is connected to the possible physics of $Tb_2Ti_2O_7$. We observe a shift in the phase boundaries with respect to those of the dipolar spin ice model as the quantum corrections become more significant. In addition to the familiar classical dipolar spin ice model phases, we see a stabilization of a $\mathbf{q} = 0$ ordered ice phase over a large part of the phase diagram − ferromagnetic correlations being preferred by quantum corrections in spite of an antiferromagnetic nearest neighbor exchange in the microscopic model. Frustration is hence seen to arise from virtual crystal field excitations over and above the effect of dipolar interactions in spin ice in inducing ice-like correlations. Our findings imply, more generally, that quantum effects could be significant in any material related to spin ices with a crystal field gap of order 100 K or smaller.

PACS numbers: 75.10.Dg, 75.10.Jm, 75.40.Cx, 75.40.Gb

I. INTRODUCTION

The problem of finding a low energy effective theory from a microscopic theory or directly from experimental considerations is a ubiquitous one in physics. The purpose is to identify the relevant degrees of freedom at some energy scale in order to capture the important physics at that scale. Often in condensed matter physics, a large separation of energy scales facilitates the process of finding an effective theory: for example in the spin ices[1,2,3] discussed below. When the separation of scales is not large, virtual (quantum mechanical) processes can become important, as in the Kondo problem in which double occupancy of the impurity in the Anderson model can be treated as a virtual process that generates the well-known s-d exchange interaction.[4] One focus of this paper is the construction of such a low energy effective theory for a highly exotic magnetic material - the $Tb_2Ti_2O_7$ pyrochlore magnetic material.

A second thread to the present work is frustration, which occurs in magnetism when interactions between spins cannot be minimized simultaneously. This happens, in the case of geometric frustration, as a consequence of the topology of the lattice. As an example, antiferromagnetic isotropic exchange interactions between classical spins on the vertices of the three dimensional pyrochlore lattice of corner-sharing tetrahedra are frustrated.[5,6,7,8,9,10] One consequence of this frustration is an extensive (macroscopic) ground state degeneracy and lack of conventional long-range order down to arbitrarily low temperatures. Theoretically, this degeneracy is expected to be lifted, partially, or fully, by other interactions,[11,12] perhaps assisted by the presence of thermal or quantum fluctuations.[7,13,14] These lessons carry over to real pyrochlore magnets in which the frustration of the principal spin-spin interaction usually manifests itself in a transition to long-range order[13,15,16,17] or a spin glass transition[18,19] well below the temperature scale set by the interactions − the Curie-Weiss temperature $\theta_{\rm CW}$. In fact, this is a ubiquitous fingerprint of highly frustrated magnets.

When short-range spin correlations persist down to arbitrarily low temperatures, as in the isotropic exchange pyrochlore antiferromagnet of Refs. 6,7, the system is referred to as a spin liquid or collective paramagnet.[5] Given the large proportion of geometrically frustrated magnetic materials which have been studied experimentally and which do ultimately exhibit an ordering transition, it does seem that spin liquids are rather rare in two and three dimensions.[20,21,22,23,24,25,26] One would expect, on general grounds, this scarcity to be particularly apparent in three dimensional materials where thermal and quantum fluctuations are the most easily quenched. This paper is concerned with the material $Tb_2Ti_2O_7$ which is one of the very few three dimensional spin liquid candidates.[26] $Tb_2Ti_2O_7$ is a pyrochlore antiferromagnet that is not magnetically ordered at any temperature above the lowest explored temperature of 50 mK,[26,27,28,29] although the Curie-Weiss temperature, $\theta_{\rm CW}$, is about −14 K, that is three hundred times larger.[30] Despite ten years[26] of experimental and

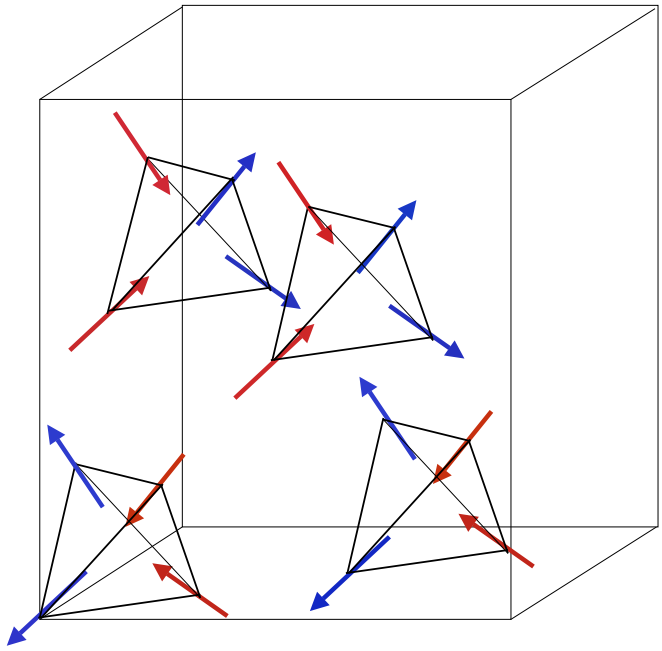

FIG. 1: (color online). Cubic unit cell of the pyrochlore lattice. The spin configuration shown is the ordered $LRSI_{001}$ state of the dipolar spin ice model.[41] The spins on each tetrahedron are aligned in the local [111] direction and satisfy the two-in/two-out ice rule.

theoretical interest in this system, the low energy magnetic properties of this material are still not currently understood.[31,32,33]

In this article, we build on earlier work[33] by presenting further evidence that qualitatively new physics, in the form of geometrical frustration, is generated via virtual crystal field excitations (VCFEs) in $Tb_2Ti_2O_7$. The frustration of interactions coming from high energies is not without precedent in condensed matter physics: frustrated exchange beyond nearest neighbor and ring exchange terms arise in small t/U effective theories derived from the Hubbard model at half-filling.[34,35,36] In this problem, the higher order terms in the effective model have only a quantitative effect on the physics which is already captured by the lowest order terms.[35]

In contrast, qualitatively new phenomena have been proposed to arise by integrating out high energies in a recent work on Mott systems,[37] and in gauge theories of frustrated magnetic systems[38,39] (which, interestingly, take as starting points models closely related to the effective model derived in Sections III and IV of this paper). The substantial effect of VCFEs on low energy physics advocated in Ref. 33 and in this article is reminiscent of the recent experimentally motivated proposal that $PrAu_2Si_2$ is a disorder-free spin glass owing to frustration dynamically arising from excited crystal field levels.[40] Before launching into the calculations, we first describe some earlier developments relating to $Tb_2Ti_2O_7$ to motivate our approach to this problem.

A. Phenomenology of $Tb_2Ti_2O_7$

There is one particular property that may be useful for making progress towards understanding the low energy physics of $Tb_2Ti_2O_7$ and which is shared by all the compounds in the $R_2M_2O_7$ family of compounds to varying degrees[10] (here R^{3+} is a rare earth ion with a magnetic crystal field ground state and M^{3+} is non-magnetic Ti^{4+} or Sn^{4+}). It is the smallness of the energy scale due to interactions, V, compared with the crystal field splitting, Δ, between the single ion ground state doublet and the first (lowest) excited states. The interactions are typically of the order of 0.1 K or smaller while the lowest crystal field splitting is of the order of tens or hundreds of Kelvin.[30,42,43] This means that the ground state wavefunction and low energy excitations mainly "live" in the Hilbert space spanned by the ground state crystal field states on all lattice sites. As we shall see in detail later on, the interactions, V, admix excited crystal field wavefunctions into the ground state doublet and these quantum corrections are weighted by $\langle V\rangle/\Delta$.[44] For the spin ices, $Ho_2Ti_2O_7$ and $Dy_2Ti_2O_7$, for which Δ is of the order of 300 K,[42] the effect of excited crystal field levels can be ignored to a very good approximation and the angular momenta can then be treated as classical Ising spins.[1,2,45] In common with the spin ices, $Tb_2Ti_2O_7$ has a crystal field ground state that can be described in terms of Ising spins.[30] But, the (classical) dipolar spin ice model (DSIM) which has, through various studies demonstrated its veracity in comparisons to the spin ices,[45,46,47] is not a good model for $Tb_2Ti_2O_7$.

An estimate of the antiferromagnetic exchange coupling in $Tb_2Ti_2O_7$ [30] puts this compound close to the phase boundary of the DSIM between the paramagnetic spin ice state (or lower temperature long-range ordered spin ice phase) and the four sublattice long-range Néel antiferromagnetic phase (see inset to Fig. 2).[41,45,48] None of these states adequately describes $Tb_2Ti_2O_7$. The long-ranged ordered phases can be ruled out on the grounds that no Bragg peaks are observed in the diffuse neutron scattering pattern.[27,28] A comparison with spin ice phenomenology is a little more subtle. One of the main features of the spin ice state is that it harbors a large residual entropy as deduced by integrating the heat capacity downwards from high temperatures.[49] Whereas, similarly to what has been observed in spin ices,[1,49] there is a broad bump in the specific heat C_V between 1 K and 2 K as the temperature is lowered, at present it remains difficult to determine whether there is a residual entropy in the collective paramagnetic state of $Tb_2Ti_2O_7$.[30,50] The study in Ref. 50 finds a slightly different heat capacity to the one in Ref. 30 and claims no evidence of residual entropy in $Tb_2Ti_2O_7$ owing to almost a complete recovery of the full entropy of the doublet-doublet crystal field levels (see also Ref. 51 for a similar finding). Instead it reports that there is a sharp feature in the heat capacity at about 300 mK indicating the onset of a glassy state. Glassiness has also been observed in the susceptibility

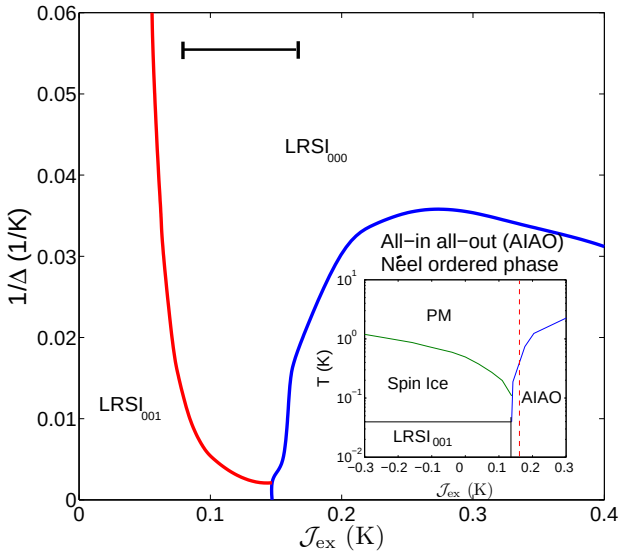

FIG. 2: (color online). Semiclassical ground state phases for the cubic unit cell model with Ewald summed dipole-dipole interactions as the crystal field gap, Δ, and the bare exchange coupling, $\mathcal{J}_{ex}$, are varied. The horizontal bar indicates a value for $1/\Delta$ ($\Delta = 18$ K) and a range of $\mathcal{J}_{ex}$ that are consistent with experimental results on $Tb_2Ti_2O_7$.[30,43] The inset is the phase diagram of the dipolar spin ice model[41,45] adopted for $Tb_2Ti_2O_7$ with $\mathcal{D} = 0.0315$ K with a vertical dotted line showing an estimated $\mathcal{J}_{ex} = 1/6$ K coupling for $Tb_2Ti_2O_7$.[30]

measurements of Ref. 52. Finally, the diffuse paramagnetic neutron scattering pattern[26,27,28,53] of $Tb_2Ti_2O_7$ differs drastically from the experimental spin ice pattern (which has been reproduced by Monte Carlo simulations of the DSIM[46] and its improvements[47]). This strongly suggests that the Ising nature of the localized moments is not an appropriate description for the magnetism in $Tb_2Ti_2O_7$, as noted in Ref. 54.

Some important insight into the microscopic nature of $Tb_2Ti_2O_7$ is provided by a mean field theory for classical spins with only a finite Ising anisotropy.[54] Specifically, Ref. 54 finds that a toy model in which spins, subject to a finite anisotropy and interacting via isotropic exchange and dipole-dipole interactions, captures the main features of the experimental paramagnetic diffuse neutron scattering pattern in $Tb_2Ti_2O_7$.[26] The results of Ref. 54 lead one to suspect that the weaker anisotropy of the spins in $Tb_2Ti_2O_7$, in contrast to those in the spin ices, can be attributed to the fact that because the ground to first excited crystal field gap is much smaller in $Tb_2Ti_2O_7$, the effect of excited crystal field states cannot be ignored. The effects of VCFEs can be studied, albeit incompletely, within the random phase approximation (RPA). A computation of the RPA diffuse neutron scattering intensity in the paramagnetic regime using the full crystal field level structure and wavefunctions[55] leads to results that are in good qualitative agreement with experiment,[27] adding weight to the idea that one of the effects of VCFEs in $Tb_2Ti_2O_7$ is to decrease the Ising anisotropy of the spins.

Having identified VCFEs as an important contribution to the physics of $Tb_2Ti_2O_7$, we look for a way of examining the effect of VCFEs on the ground state of perhaps the simplest minimal model for $Tb_2Ti_2O_7$. An approach that is well-suited to this problem is an effective Hamiltonian formalism. The low energy theory that is obtained within this formalism inhabits a product of two dimensional Hilbert spaces − one for each magnetic site − spanned by the ground state crystal field doublet. So, the effective theory can be written in terms of (pseudo) spins one-half. Neglecting VCFEs, the effective Hamiltonian is simply the theory obtained by projecting onto the ground state crystal field doublet on each magnetic ion which, as we shall see, is the DSIM of interacting (classical) Ising spins i.e. a model in which transverse spin fluctuations are absent.[2] The separation of energy scales to which we have alluded then allows us to develop a perturbation series in the parameter $\langle V\rangle/\Delta$ [44] where the zeroth order term is the DSIM [2] and higher order terms explicitly incorporate the effect of VCFEs in terms of operators acting within the projected Hilbert space. The procedure can be written schematically as

$$H(\mathbf{J}) = H_{\rm cf} + V \xrightarrow[\text{perturbation theory}]{\text{projection}} H_{\rm eff}(\mathbf{S}_{\rm eff})$$

where the bare microscopic Hamiltonian H, depending on magnetic moments $\mathbf{J}$ through the crystal field $H_{\rm cf}$ and interactions V, is used to derive an effective Hamiltonian $H_{\rm eff}$ in terms of pseudospins 1/2, $\mathbf{S}_{\rm eff}$.

One advantage of this approach is that, by decreasing $\langle V\rangle/\Delta$, we can smoothly connect our results to the physics of spin ice.[1,2,3] A second more practical advantage is that, since the dimensionality of the relevant Hilbert space is reduced, exact diagonalization calculations on finite size clusters (albeit small clusters), series expansion techniques and the linked cluster method may become tractable.[56]

A comparison has previously been made[33] between the effective Hamiltonian to lowest order in quantum corrections, $\langle\mathcal{J}_{ex}\rangle/\Delta$, with the crystal field gap Δ as a free parameter and the "high energy" microscopic (bare) model from which it was obtained. This involved an exact diagonalization of the two models on a single tetrahedron to determine the ground state as a function of Δ and the exchange coupling.[33] The result is shown in Fig. 3. The ground state degeneracies largely coincide over the range of parameters explored, which includes the estimated exchange coupling of $Tb_2Ti_2O_7$. Most importantly, in the singlet region of the phase diagram, the ground state of the exact bare microscopic model is a nondegenerate superposition of states each satisfying the spin ice constraint. In contrast, for the classical dipolar ice model with the same exchange coupling, on a single tetrahedron and on a lattice, the ground state is a

doubly degenerate all-in/all-out state (see Fig. 14(a)). That the full quantum problem favors spin ice-like correlations at the single tetrahedron level was shown to arise from a renormalization of the Ising exchange in the effective anisotropic spin-1/2 Hamiltonian when VCFEs are included.[33] Finally, it was found that the level structure from exact diagonalization of the original model on a single tetrahedron is sufficient to reproduce the main semi-quantitative features of the experimental diffuse neutron scattering pattern for $Tb_2Ti_2O_7$.[33]

The renormalization of the effective nearest neighbor Ising exchange by VCFEs such that spin ice correlations are energetically preferred over a larger range of the bare exchange couplings than would be the case without quantum corrections shows clearly that quantum effects can have a significant effect on the nature of the correlations in $Tb_2Ti_2O_7$. However, owing to the presence of a long-range dipole-dipole interaction and the fact that VCFEs in themselves generate interactions beyond nearest neighbor, it was not clear on the basis of earlier work[33] whether VCFEs would have a significant, or even the same qualitative effect on the $Tb_2Ti_2O_7$ correlations when considering the full lattice. That is the main problem that we resolve in this work.

B. Scope of the paper

In this article, we present a more detailed derivation of the effective Hamiltonian for $Tb_2Ti_2O_7$ than was possible in the earlier work[33] owing to lack of space. We also take some initial steps beyond the single tetrahedron approximation by calculating the ground states of the effective model assuming that the effective $S_{\rm eff} = 1/2$ spins are classical spins of fixed length (large S approximation). Our main result is shown in Fig. 2 which is discussed more fully in Section V D. The plot shows the semi-classical phase diagram of the effective model on a cubic unit cell with periodic boundary conditions as a function of the gap Δ and the isotropic exchange coupling $\mathcal{J}_{\rm ex}$ in the microscopic model. When $1/\Delta = 0$, all quantum corrections are suppressed and we recover the limit of the dipolar spin ice model (DSIM) with two phases - a state with the spin ice rule satisfied on each tetrahedron and ordering wavevector 001 ($\rm LRSI_{001}$) and a four-in/four-out Ising state (AIAO) for more antiferromagnetic $\mathcal{J}_{\rm ex}$. Compared to the dipolar spin ice model ground states, the effective model contains one other phase − a $\mathbf{q} = 0$ long range ordered spin ice phase ($\rm LRSI_{000}$). Also, the magnetic moments in the $\rm LRSI_{000}$ and $\rm LRSI_{001}$ phases are canted away from the local Ising directions as Δ decreases. The region over which the $\rm LRSI_{000}$ is the ground state forms a wedge, broadening out to lower Δ until it is the only phase found within the explored range of $\mathcal{J}_{\rm ex}$ at the expense of the antiferromagnetic AIAO phase. There are two main physical mechanisms (contributions) to the stabilization of the $\rm LRSI_{000}$ state across the phase diagram. The first is that the effective nearest neighbor Ising coupling becomes more ferromagnetic in character as Δ decreases. However, it does eventually change sign as $\mathcal{J}_{\rm ex}$ increases over the entire range of Δ studied. So the second reason for the spreading of a spin ice state across the phase diagram as Δ decreases is due to beyond nearest neighbor interactions that arise purely from effective VCFEs and which monotonically increase in strength as Δ decreases.

The outline of the paper is as follows. In Section II, we introduce some notation and describe the micro-

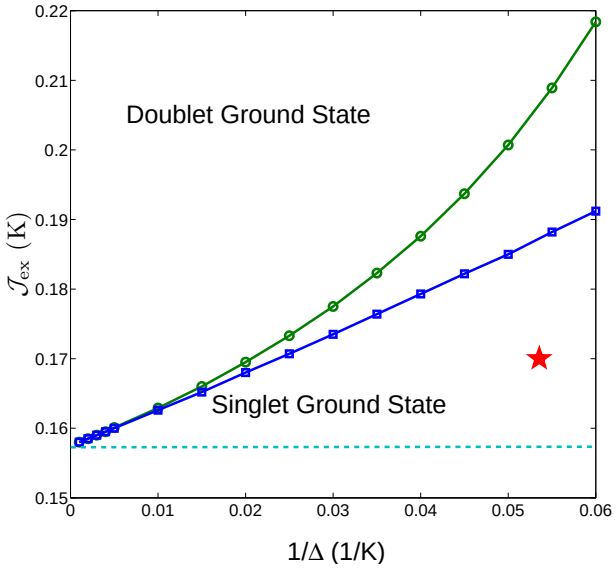

FIG. 3: (color online). Figure showing exact diagonalization of a minimal Hamiltonian, $H = H_{\rm cf} + V$, on a single tetrahedron. The ground state degeneracy is shown for different values of the ground-to-first excited crystal field gap Δ, and the bare exchange coupling $\mathcal{J}_{\rm ex}$ for fixed dipolar strength $\mathcal{D} = 0.0315$ K relevant to $Tb_2Ti_2O_7$. There are two regions: one with a singlet ground state, the other with a doubly degenerate ground state. The boundary between the two regions is marked for the two models considered. For the effective Hamiltonian the boundary is marked by circles and for the four crystal field state microscopic model on a single tetrahedron described in the main text (based on the crystal field Hamiltonian Eq. (27)), the boundary is traced out by squares. For the estimated parameters $(\mathcal{J}_{\rm ex}, D, \Delta)$ for $Tb_2Ti_2O_7$, indicated by a star, the boundaries agree to within ten percent. The horizontal dashed line shows the phase boundary of the classical part ($1/\Delta = 0$) of the effective Hamiltonian between the all-in/all-out doublet configurations and sextet (degenerate two-in/two-out) "spin ice" ground states. Within the classical description, $Tb_2Ti_2O_7$ would be in the doublet all-in/all-out state (i.e. above the horizontal dashed line). However, when VCFEs are included, the phase boundary is shifted towards larger (i.e. more antiferromagnetic) values of the bare exchange in such a way that $Tb_2Ti_2O_7$ "finds itself" below the boundary in a singlet ground state. The singlet arises because of fluctuations that lift the sixfold degeneracy of classical two-in/two-out configurations on a single tetrahedron.

scopic (bare) model for $Tb_2Ti_2O_7$ from which the effective model is derived. With this in hand, we formulate our approach in more detail than in this introduction. Section III discusses the form and properties of the lowest order (classical dipolar spin ice) term in the effective Hamiltonian. In Section IV, the quantum corrections to this model are enumerated to lowest order in $\langle V\rangle/\Delta$ and we study how the longitudinal (Ising) exchange coupling in the dipolar spin ice model (DSIM) is renormalized to this order. Having obtained the effective Hamiltonian for $Tb_2Ti_2O_7$ to lowest order in the $1/\Delta$, we treat the effective $S = 1/2$ spins as classical spins and present, in Section V, the resulting semiclassical ground states. This study of the ground states allows us to see how the effect of VCFEs is connected to the physics of spin ice and also clearly shows that spin ice correlations are present even though the bare microscopic exchange coupling $\mathcal{J}_{\rm ex}$ is antiferromagnetic.

> *In other words, geometric frustration in the model (Eqs. (1),(2) and (5)) of $Tb_2Ti_2O_7$ emerges from quantum virtual crystal field excitations (VCFEs) and many-body physics.*

This is the main result of our paper. We discuss these results, in Section VI, in the light of experiments on $Tb_2Ti_2O_7$ and describe some possible further applications of the effective Hamiltonian that we derive for $Tb_2Ti_2O_7$. Finally, we provide in Appendix A, details of the effective Hamiltonian method as a background to the main application to $Tb_2Ti_2O_7$ described in the remainder of the paper. Appendix B contains further details behind the calculations presented in Section IV and Appendix C gives some data used to convert between crystal field parameters for different rare earth pyrochlore titanates using a point charge approximation.

We note here that while our specific focus is on the $Tb_2Ti_2O_7$ pyrochlore magnet, the formalism that we employ below could be straightforwardly used to construct effective low energy theories for many other frustrated rare earth systems where the excited crystal field levels have a somewhat larger energy scale than the microscopic interactions.

II. EFFECTIVE HAMILTONIAN

A. Microscopic (Bare) Model

The microscopic or bare Hamiltonian for the magnetic Tb^{3+} ions in $Tb_2Ti_2O_7$ is given by

$$H = H_{\rm cf} + V \tag{1}$$

where $H_{\rm cf}$ is the crystal field Hamiltonian and V are the interactions between the ions. In the remainder of this section we explain the form of both terms in some detail.

The magnetic Tb^{3+} ions in $Tb_2Ti_2O_7$ are arranged on the sites of a pyrochlore lattice. The pyrochlore lattice consists of corner-shared tetrahedra which can otherwise be thought of as a face-centered cubic (fcc) lattice with primitive translation vectors $\mathbf{R}_A$ for $A = 1, 2, 3$ and a basis of four ions $\mathbf{r}^a$ ($a = 1, \ldots, 4$). We follow the same labeling of the four sublattice basis vectors as in Ref. 54. It is useful to introduce a coordinate system on each of the four sublattices with local $\hat{\mathbf{z}}^a$ unit vector along the local cubic [111] direction. The sublattice basis vectors and local Cartesian $\hat{\mathbf{x}}^a$, $\hat{\mathbf{y}}^a$ and $\hat{\mathbf{z}}^a$ directions are given in Table I. Below, we also make use of rotation matrices $u^a_{\alpha\beta}$ (the elements of which are contained in Table I) which achieve a passive transformation that takes the local sublattice coordinate system for sublattice a into the global Cartesian laboratory axes.

Spin-orbit coupling within the relevant localized $4f$ levels of the Tb^{3+} ions leaves total angular momentum $\mathbf{J}$ as a good quantum number with J = 6. The local environment about each Tb^{3+} ion is responsible for breaking the $2J + 1$ degeneracy. Its effect can be computed from a crystal field Hamiltonian, $H_{\rm cf}$, which is constrained by symmetry to take the form[30,42,43]

$$H_{\rm cf} = \sum_{i,a} B^0_2 O^0_2(i,a) + B^0_4 O^0_4(i,a) + B^3_4 O^3_4(i,a) + B^0_6 O^0_6(i,a) + B^3_6 O^3_6(i,a) + B^6_6 O^6_6(i,a). \tag{2}$$

The magnetic ions are labeled by an fcc site i and a sublattice index a. Expressions for the operators O^m_l in terms of the local angular momentum components can be found, for example, in Hutchings.[57] The crystal field in $Tb_2Ti_2O_7$ has been studied in Refs. 30 and 43 resulting in somewhat differing estimates for the parameters B^m_l. In the following, all quantitative results that we present for $Tb_2Ti_2O_7$ were obtained using crystal field parameters for $Ho_2Ti_2O_7$, obtained from inelastic neutron scattering in Ref. 42, which have been rescaled to the $Tb_2Ti_2O_7$ parameters according to

$$(B^m_l)_{\rm Tb} = \left(\frac{(S_l)_{\rm Tb}}{(S_l)_{\rm Ho}}\right)\left(\frac{\langle r^m\rangle_{\rm Tb}}{\langle r^m\rangle_{\rm Ho}}\right)(B^m_l)_{\rm Ho}. \tag{3}$$

Here, the S_l are Stevens factors.[58] These and the radial expectation values $\langle r^m\rangle$ for the rare earth ions[59] can be found in Appendix C. We have checked that using the crystal field parameters of Ref. 43 instead leads to results that are in fairly close quantitative agreement with those obtained using the rescaled parameters from Eq. (3).

The crystal field Hamiltonian, $H_{\rm cf}$, can be diagonalized numerically exactly; the eigenvalues are E_n and the eigenstates $|n\rangle$ for $n = 1, \ldots, 13$, which we implicitly arrange in order of increasing energy. One finds a level structure that includes a ground state and a first excited state that are both doubly degenerate.[30,43] The splitting, Δ, between the ground and first excited states is about 18.6 K,[30,43] which is much smaller than the corresponding gap in the spin ices (for example, the gap in $Ho_2Ti_2O_7$ is about 230 K [42]). It is the smallness of this value of Δ compared to V for $Tb_2Ti_2O_7$ and the possibility of admixing between the ground state and excited state crystal

TABLE I: Basis of four magnetic ions on a pyrochlore indexed by position vectors $\mathbf{r}^a$. The local [111] direction on each sublattice is $\mathbf{z}^a$. The edge length of the cubic unit cell is a. The rotation matrix $u^a_{\alpha\beta}$ takes the form $(\mathbf{x}^a, \mathbf{y}^a, \mathbf{z}^a)^T_{\alpha\beta}$ in which the vector components are placed in the matrix columns. In the main text, we make use of vectors $\hat{\mathbf{n}}^x = (1,0,0)$,$\hat{\mathbf{n}}^y = (0,1,0)$,$\hat{\mathbf{n}}^z = (0,0,1)$ in the laboratory coordinate system.

Sublattice	$\mathbf{r}^a$	$\mathbf{x}^a$	$\mathbf{y}^a$	$\mathbf{z}^a$
1	$(a/4)(0,0,0)$	$(1/\sqrt{6})(-1,-1,2)$	$(1/\sqrt{2})(1,-1,0)$	$(1/\sqrt{3})(1,1,1)$
2	$(a/4)(1,1,0)$	$(1/\sqrt{6})(1,1,2)$	$(1/\sqrt{2})(-1,1,0)$	$(1/\sqrt{3})(-1,-1,1)$
3	$(a/4)(1,0,1)$	$(1/\sqrt{6})(1,-1,-2)$	$(1/\sqrt{2})(-1,-1,0)$	$(1/\sqrt{3})(-1,1,-1)$
4	$(a/4)(0,1,1)$	$(1/\sqrt{6})(-1,1,-2)$	$(1/\sqrt{2})(1,1,0)$	$(1/\sqrt{3})(1,-1,-1)$

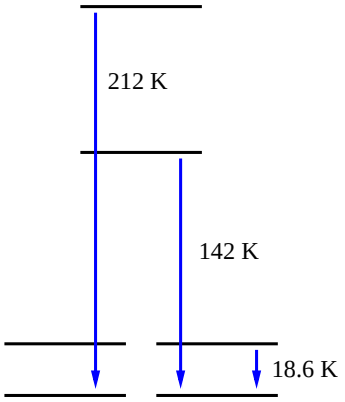

FIG. 4: (color online). Figure indicating the four lowest levels of the crystal field spectrum (not to scale). The splitting between the ground state doublet and the first excited state is called Δ. The ground state and the first excited state are doublets.[30] The two other excited states are singlets.[30]

field levels that are at the root of all the phenomenology that we explore in the rest of this paper. Fig. 4 shows the level structure of the crystal field spectrum for the four lowest levels determined on the basis of an exact diagonalization of Eq. (2).

We emphasize two features of this spectrum that will be important later on. First of all, let us write down the time reversal properties of the eigenstates, $|n\rangle$. Let $|n\rangle$ be written as a linear combination of the eigenstates of $\mathbf{J}$, denoted $|\mathrm{J}, M\rangle$,

$$|n\rangle = \sum_M c_n^M |\mathrm{J}, M\rangle.$$

Time reversal invariance requires that the coefficients are related to one another by $c_n^M = (-)^{J-M} c_n^{-M}$.[60] Secondly, it is possible to interpret the non-interacting single ion angular momenta as Ising-like at low energies, as was done in Ref. 45. This is because, at sufficiently low energies, thermal occupation of excited crystal field levels is negligible and one can focus on the ground state doublet. The ground state doublet states, $|1\rangle$ and $|2\rangle$, have

$$\langle 1|\widetilde{\mathrm{J}}^z|1\rangle = -\langle 2|\widetilde{\mathrm{J}}^z|2\rangle \equiv \langle \widetilde{\mathrm{J}}^z\rangle \tag{4}$$

as the only nonvanishing matrix elements, where the tilde indicates that the z axis is taken along the local [111] direction appropriate to each magnetic ion (see Table I). So, this doublet considered on its own has nonzero angular momentum expectation values only along one axis with vanishing transition matrix elements $\langle 1|\widetilde{\mathrm{J}}^{\pm}|2\rangle = 0$.

The interactions between the angular momenta, $V \equiv H_{\rm ex} + H_{\rm dd}$, are taken to be nearest neighbor isotropic exchange $H_{\rm ex}$ and dipole-dipole interactions, $H_{\rm dd}$:

$$H_{\rm ex} = \mathcal{J}_{\rm ex} \sum_{\langle (i,a),(j,b)\rangle} \mathbf{J}_{i,a}\cdot\mathbf{J}_{j,b}$$
$$H_{\rm dd} = \mathcal{D} r_{\rm nn}^3 \sum_{\rm pairs} \frac{\mathbf{J}_{i,a}\cdot\mathbf{J}_{j,b}}{|\mathbf{R}_{ij}^{ab}|^3} - 3\frac{(\mathbf{J}_{i,a}\cdot\mathbf{R}_{ij}^{ab})(\mathbf{J}_{j,b}\cdot\mathbf{R}_{ij}^{\rm ab})}{|\mathbf{R}_{ij}^{ab}|^5}. \tag{5}$$

The notation $\mathbf{R}_{ij}^{ab}$ is short for $\mathbf{R}_i^a - \mathbf{R}_j^b$ with $\mathbf{R}_i^a = \mathbf{R}_i + \mathbf{r}^a$ and $r_{\rm nn} = 3.59\mathring{A} = a\sqrt{2}/4$ (where a is the edge length of the conventional cubic unit cell) is the distance between neighboring magnetic ions.[30] Here, we employ the convention that $\mathcal{J}_{\rm ex} > 0$ is antiferromagnetic and $\mathcal{J}_{\rm ex} < 0$ is ferromagnetic. This is the simplest Hamiltonian consistent with the nonvanishing Tb^{3+} dipole-dipole coupling, $\mathcal{D} = (\mu_0/4\pi)(g_J\mu_B)^2/r_{\rm nn}^3 = 0.0315$ K with the Landé factor, $g_J = 3/2$ and with the negative Curie-Weiss temperature $\theta_{\rm CW} = -14$ K.[30] The exchange coupling $\mathcal{J}_{\rm ex}$ has been estimated from $\theta_{\rm CW}$ for $Tb_2Ti_2O_7$ and $\theta_{\rm CW}$ for the diluted compound $(Y_{0.98}Tb_{0.02})_2Ti_2O_7$ [30] to be about 0.17 K, while a fit in Ref. 43 gives a value for $\mathcal{J}_{\rm ex} = 0.083$ K that is significantly less antiferromagnetic.[61]

In summary, our bare microscopic model for $Tb_2Ti_2O_7$ consists of three terms: the crystal field Hamiltonian $H_{\rm cf}$, an isotropic exchange $H_{\rm ex}$ with an antiferromagnetic coupling and a dipole-dipole interaction, $H_{\rm dd}$.[62] An extension of the present work could include (i) bare exchange couplings beyond nearest neighbors, (ii) anisotropic nearest neighbor exchange as described in Ref. 63 and (iii) direct or virtual (phonon-mediated) multipolar interactions.[64]

B. Route to an effective Hamiltonian

If we were able to ignore the excited crystal field levels in $Tb_2Ti_2O_7$, the angular momenta could be treated

as classical Ising spins[2,45] because the only nonvanishing matrix elements of the angular momentum are those in Eq. (4).[2] However, for reasons outlined in the Introduction, this is not a good approximation for this material. The interactions between the angular momenta induce VCFEs that admix excited crystal field wavefunctions into the space spanned by the non-interacting crystal field doublets with the consequence that the magnetic moments behave much less anisotropically than one would expect on the basis of the [111] Ising-like ground state crystal field doublet. These quantum fluctuations can be treated perturbatively because there is a small dimensionless parameter $\langle V\rangle/\Delta$, where $\langle V\rangle \sim O(\max(\mathcal{J}_{\rm ex},\mathcal{D}))$. To lowest order in such a perturbation theory, and in a low energy effective model, the spins should be perfectly Ising-like and hence we recover the DSIM. We now proceed to make these ideas more concrete.

Because we seek a Hamiltonian operating within a low energy subspace, we need a projection operator onto the non-interacting single ion crystal field ground states. For a single ion at the site specified by indices i, a, the projection is accomplished by

$$\mathcal{P}(i,a) = |1_{i,a}\rangle\langle 1_{i,a}| + |2_{i,a}\rangle\langle 2_{i,a}|.$$

This operator satisfies the conditions $\mathcal{P}^2(i,a) = \mathcal{P}(i,a)$ and Hermiticity. With moments on all the sites of the lattice, the projector is $\mathcal{P} \equiv \prod_{i,a} \mathcal{P}(i,a)$. The subspace of the full Hilbert space selected by the projector will be called the model space, $\mathfrak{M} \equiv \prod_{\otimes(i,a)} \mathfrak{M}_{i,a}$, from now on. The Hilbert space $\mathfrak{M}_{i,a}$ is defined as the space spanned by states $|1_{i,a}\rangle$ and $|2_{i,a}\rangle$ on site (i,a).

The spin-spin interaction

$$V \equiv H_{\rm ex} + H_{\rm dd} \tag{6}$$

is to be treated as a perturbation. Because the perturbation V is "small" compared to the difference between the ground and first excited crystal field energies Δ, $H_{\rm cf} \equiv H_0$, we expect that on a crystal of N sites, the 2^N lowest energy eigenstates of H lie mainly within $\mathfrak{M}$ because the admixing of excited crystal field wavefunctions into the model space is a small effect. Our effective Hamiltonian will be defined in such a way that its eigenstates live entirely within $\mathfrak{M}$ while its eigenvalues exactly correspond to the 2^N lowest energy eigenvalues of the exact Hamiltonian, H. The 2^N lowest energy eigenstates of H mainly lie within $\mathfrak{M}$ in the sense that the rotation of exact states out of the model space is determined by the relatively small perturbation $\langle V\rangle/\Delta$.

In practice, the exact eigenvalues can be approximated by carrying out perturbation theory in the construction of the effective Hamiltonian $H_{\rm eff}$. After some work, that is briefly laid out in Appendix A, one finds that the effective Hamiltonian can be written as[65]

$$H_{\rm eff} = \mathcal{P}H_0\mathcal{P} + \mathcal{P}V\mathcal{P} + \mathcal{P}V\mathcal{R}V\mathcal{P} + \ldots \tag{7}$$

The operator $\mathcal{R}$ − the resolvent operator− is given by

$$\mathcal{R} = \sum_{|P\rangle\notin\mathfrak{M}} \frac{|P\rangle\langle P|}{E_g - E_P} \tag{8}$$

where, for a finite crystal of N sites, E_g is N times the energy of the degenerate ground state crystal field levels E_0. The numerator of each term in the resolvent is a projector onto a space orthogonal to $\mathfrak{M}$ − a product of crystal field operators $|P\rangle\langle P| \equiv \prod_{\otimes} |n\rangle\langle n|$ where the product is taken over all sites of the lattice with at least one such operator having $n > 2$ (i.e. belonging to the group of excited crystal field states); this is the meaning of the notation $|P\rangle \notin \mathfrak{M}$ in the summation index of Eq. (8). The third term on the right-hand-side of Eq. (7) is the lowest order term in the perturbation series to include the effects of crystal field states outside the model space. This term is therefore the lowest order contribution of the VCFEs that we have referred to above.

Equation (7) makes no reference to a particular model. In Sections III and IV, we develop the terms in the effective Hamiltonian for the model $H = H_0 + V \equiv H_{\rm cf} + H_{\rm dd} + H_{\rm ex}$ of $Tb_2Ti_2O_7$ described in Section II A. Section III is devoted to the lowest order, or classical, term $\mathcal{P}H\mathcal{P}$. Section IV enumerates the lowest order terms generated by VCFEs, relating each underlying class of terms that originate from $\mathcal{P}H\mathcal{R}H\mathcal{P}$ to specific virtual excitation channels. Higher order corrections than $\mathcal{P}H\mathcal{R}H\mathcal{P}$ are computationally difficult to determine mainly because of the presence of the long-range dipole interactions $H_{\rm dd}$. See Ref. 66 for a model on a pyrochlore for which degenerate perturbation theory can be carried out to much higher order than is done is this work.

To spare readers the details of this rather technical derivation if they so choose, we include a short summary (Section IV F) of the form of the low energy model for $Tb_2Ti_2O_7$. Finally, in Section IV G, we summarize some results that have been obtained from the effective Hamiltonian which have already appeared in the literature.[33,67] All in all, we shall see that the DSIM couplings are renormalized by VCFEs and that effective anisotropic spin-spin couplings appear in addition to the Ising interactions of the DSIM. In other words, the effective theory allows for fluctuations of the moments perpendicular to the local $\mathbf{z}^a$ axes. We shall study the variation of the effective couplings in $H_{\rm eff}$ as $\mathcal{J}_{\rm ex}$ is varied. This information will be useful in the interpretation of the semiclassical ground states of the effective model (Section V) and hence in assessing the effects of VCFEs on the physics of $Tb_2Ti_2O_7$.

III. CLASSICAL PART OF $H_{\rm eff}$

A. [111] Ising model for $Tb_2Ti_2O_7$

In this subsection, we consider the (lowest order) term $\mathcal{P}H\mathcal{P}$ in Eq. (7). The effective Hamiltonian derived from H for $Tb_2Ti_2O_7$ can be rendered in the form of a spin

one-half model by rewriting the model space operators in Eq. (7) in terms of Pauli matrices. This is possible because the model space, in our case, is a direct product of two dimensional Hilbert spaces spanned by the ground state crystal field doublet. The correspondence between Pauli matrices and operators on the crystal field ground state:

$$\tilde{\sigma}^x = |1\rangle\langle 2| + |2\rangle\langle 1| \tag{9}$$

$$\tilde{\sigma}^y = -i(|1\rangle\langle 2| - |2\rangle\langle 1|) \tag{10}$$

$$\tilde{\sigma}^z = |1\rangle\langle 1| - |2\rangle\langle 2| \tag{11}$$

together with the unit operator $\mathbb{I} = |1\rangle\langle 1| + |2\rangle\langle 2|$. Note, however, that despite the fact they do satisfy the commutation rules

$$[\tilde{\sigma}^\alpha, \tilde{\sigma}^\beta] = 2i\epsilon_{\alpha\beta\gamma}\tilde{\sigma}^\gamma,$$

where $\epsilon_{\alpha\beta\gamma}$ is the Levi-Civita symbol, the $\tilde{\sigma}^\alpha$ do not swap sign under time reversal so they are not true angular momentum operators. For this reason, we shall call them pseudospins or effective spins. It is helpful for later sections to give their properties under $\mathfrak{T}$, the time reversal transformation:

$$\mathfrak{T} : \tilde{\sigma}^x \to \tilde{\sigma}^x \tag{12}$$

$$\mathfrak{T} : \tilde{\sigma}^y \to \tilde{\sigma}^y \tag{13}$$

$$\mathfrak{T} : \tilde{\sigma}^z \to -\tilde{\sigma}^z \tag{14}$$

because $\mathfrak{T} : |1(2)\rangle \to |2(1)\rangle$.

If we apply the projector to the full Hamiltonian to obtain $\mathcal{P}H\mathcal{P}$, we find that the crystal field part $H_{\rm cf}$ becomes $E_0 \sum_{i,a} \mathbb{I}_{i,a}$ with $E_1 = E_2 \equiv E_0$. From now on, we omit this constant energy shift. To project the interaction part $\mathcal{P}V\mathcal{P}$, we write the angular momentum components in the local coordinate system with local $\hat{\mathbf{z}}^a$ axes in the directions given in Table I: $J^\alpha_{i,a} = u^a_{\alpha\beta}\widetilde{J}^\beta_{i,a}$. All operator components that refer to the local coordinate systems are labeled with a tilde. Also, when it is not important to distinguish different sublattices, we abbreviate (i, a) with the site index I. We add further numerical subscripts to I to label different sites. With this notation, the projector acting on $\widetilde{J}^z_I$ gives

$$\langle\widetilde{J}^z_I\rangle(|1_I\rangle\langle 1_I| - |2_I\rangle\langle 2_I|) = \langle\widetilde{J}^z_I\rangle\tilde{\sigma}^z_I$$

where $\langle\widetilde{J}^z_I\rangle = \langle 1|\widetilde{J}^z|1\rangle$. Owing to $\langle 1|\widetilde{J}^\pm|2\rangle = 0$, all matrix elements of the other angular momentum components vanish. So, the isotropic exchange $H_{\rm ex}$ becomes

$$\mathcal{P}H_{\rm ex}\mathcal{P} = \mathcal{J}_{\rm classical} \sum_{\langle I_1, I_2\rangle} (\hat{\mathbf{z}}^a \cdot \hat{\mathbf{z}}^b)\tilde{\sigma}^z_{I_1}\tilde{\sigma}^z_{I_2} \tag{15}$$

and the dipole-dipole interaction becomes

$$\mathcal{P}H_{\rm dd}\mathcal{P} = \mathcal{D}_{\rm classical} r^3_{\rm nn} \times \frac{1}{2}\sum_{(i,a;j,b)} \left(\frac{(\hat{\mathbf{z}}^a \cdot \hat{\mathbf{z}}^b)}{|\mathbf{R}^{ab}_{ij}|^3} - 3\frac{(\hat{\mathbf{z}}^a \cdot \mathbf{R}^{ab}_{ij})(\hat{\mathbf{z}}^b \cdot \mathbf{R}^{ab}_{ij})}{|\mathbf{R}^{ab}_{ij}|^5} \right) \tilde{\sigma}^z_{i,a}\tilde{\sigma}^z_{i,b}. \tag{16}$$

The renormalized, or effective, exchange and dipole-dipole couplings are, respectively, $\mathcal{J}_{\rm classical} = \mathcal{J}_{\rm ex}\langle\widetilde{J}^z\rangle^2$ and $\mathcal{D}_{\rm classical} = \mathcal{D}\langle\widetilde{J}^z\rangle^2$. $H_{\rm DSM} = \mathcal{P}(H_{\rm ex} + H_{\rm dd})\mathcal{P}$ is the celebrated DSIM.[1,2,3,41,45,47,68] It is a classical (local Ising) model because all the terms mutually commute as they solely consist of $\tilde{\sigma}^z_{i,a}$ operators. This model exhibits two different ground states depending on the ratio of the exchange to the dipolar coupling; these are shown in the inset of Fig. 2. When $\mathcal{J}_{\rm ex}/\mathcal{D} > 4.525$, the ground state has ordering wavevector $\mathbf{q} = 0$ with the spins on a single tetrahedron in the $|1\rangle$ state or the $|2\rangle$ state − the all-in/all-out phase.[45] When $\mathcal{J}_{\rm ex}/\mathcal{D} < 4.525$, the ordering wavevector of the ground state is $(0, 0, 2\pi/a)$ and each tetrahedron has spins satisfying the two-in/two-out ice rule; we refer to this state as the $\rm LRSI_{001}$ phase,[1,41,48] with one of the domains shown in Fig. 1.[69] Above a nonzero critical temperature, the $\rm LRSI_{001}$ phase gives way[1] to a spin ice state with no conventional long-range order (Fig. 2).

Formally speaking, the spin ice state is a collective paramagnetic state[5] − a classical spin liquid of sorts. That the DSIM has proved to be a good model for spin ice materials is largely due to the substantial gap Δ between the crystal field ground state doublet and first excited state which results in a roughly $1/\Delta$ suppression of VCFEs.[70] This model is not a good description for $Tb_2Ti_2O_7$. Indeed, if we consider the estimated couplings given in Section II A, we find $\mathcal{J}_{\rm ex}/\mathcal{D} \sim 5.4$ (recalling $\mathcal{J}_{\rm ex} \approx 0.17$ K and $\mathcal{D} \approx 0.0315$ K as stated in Section II A), which would put $Tb_2Ti_2O_7$ in the all-in/all-out phase with a critical temperature into this phase from the paramagnetic phase at $T_c \sim 0.5$ K (see vertical dashed line in the inset to Fig. 2).[45] This is in contradiction with neutron scattering experiments which find no magnetic Bragg peaks in zero field.[71] If we allow for inaccuracies in the estimate of $\mathcal{J}_{\rm ex}$,[43,71] such that a classical, dipolar spin ice state is implied by the coupling, we find various properties of spin ices that are not compatible with those of $Tb_2Ti_2O_7$. Some of these conflicting properties − the diffuse neutron scattering pattern and differing spin anisotropies − were discussed in the Introduction. Therefore, in the next section, we investigate what happens when Δ is small enough that the lowest order fluctuation term $\mathcal{P}H\mathcal{R}H\mathcal{P}$ in Eq. (7) becomes important.

B. Exchange convention

In Eq. (5), we use the opposite sign convention for the exchange coupling to the one used in Refs. 41, 45 and 48.[69] The convention in these works is to include a minus sign in front of the exchange coupling in contrast to our Eq. (5). In this article, in the global coordinate system, antiferromagnetic corresponds to $\mathcal{J}_{\rm ex} > 0$.

A warning must be made regarding the convention within the local coordinate system. In rotating to the local system, geometrical factors appear in front of the

couplings. For example, as shown in Section III, the local Ising exchange part of the coupling $\mathcal{J}_{\rm ex}\mathbf{J}_{i,a}\cdot\mathbf{J}_{j,b}$ is $\mathcal{J}_{\rm ex}(\hat{\mathbf{z}}^a\cdot\hat{\mathbf{z}}^b)\tilde{J}_{i,a}\cdot\tilde{J}^z_{j,b}$ where $(\hat{\mathbf{z}}^a\cdot\hat{\mathbf{z}}^b)=-1/3$ arises from the fact that the local $\hat{\mathbf{z}}$ axes are not collinear. In the following pages, we adopt the simplifying scheme of absorbing the geometrical factors into the couplings. In doing so, it will be useful to describe how to go from the sign of the local effective Ising coupling, J^{zz}, in front of $J^{zz}\tilde{\sigma}^z\tilde{\sigma}^z$ to the type of order that is energetically favored by the coupling. Thus, when the local coupling is said to be ferromagnetic, J^{zz} is negative and the Ising components of the spins prefer to lie in an all-in/all-out configuration. When, instead, J^{zz} is positive, it is said to be antiferromagnetic and the local Ising components are frustrated, leading to a spin ice configuration on each tetrahedron.

IV. LOWEST ORDER QUANTUM FLUCTUATIONS

A. General Considerations

In this section we present a derivation of the quantum terms $\mathcal{PVRVP}$ in the effective Hamiltonian. We refer those readers interested only in the results of this technical derivation to Section IV F. We begin by introducing a little more notation to describe the structure of the term $\mathcal{PVRVP}$ which we shall refer to as $H^{(2)}_{\rm eff}$. We write the interaction term V in the form

$$\begin{aligned} V&=\sum_{I_1,I_2}\sum_{\alpha,\beta}\mathcal{K}^{\alpha,\beta}_{I_1I_2}J^\alpha_{I_1}J^\beta_{I_2}\\ &=\sum_{I_1,I_2}\sum_{\alpha,\beta}\tilde{\mathcal{K}}^{\alpha,\beta}_{I_1I_2}\tilde{J}^\alpha_{I_1}\tilde{J}^\beta_{I_2}\end{aligned}\tag{17}$$

where, in the second line, we have absorbed the rotation matrices $u^a_{\alpha\beta}$ into the definition of $\tilde{\mathcal{K}}$. When the spins interact via nearest neighbor isotropic exchange and long-ranged dipole-dipole interactions as in Eq. (5), we have for $\mathcal{K}$:

$$\begin{aligned}\mathcal{K}^{\alpha,\beta}_{(i,a),(j,b)}&=\frac{1}{2}\mathcal{J}_{\rm ex}\delta_{\mathbf{R}^{ab}_{ij},r_{\rm nn}}(\mathbf{n}^\alpha\cdot\mathbf{n}^\beta)\\&+\frac{1}{2}\mathcal{D}r^3_{\rm nn}\left(\frac{(\mathbf{n}^\alpha\cdot\mathbf{n}^\beta)}{|\mathbf{R}^{ab}_{ij}|^3}-3\frac{(\mathbf{n}^\alpha\cdot\mathbf{R}^{ab}_{ij})(\mathbf{n}^\beta\cdot\mathbf{R}^{ab}_{ij})}{|\mathbf{R}^{ab}_{ij}|^5}\right).\end{aligned}\tag{18}$$

with unit vectors $\mathbf{n}^\alpha$ for $\alpha=x,y,z$ in the laboratory x,y,z directions respectively (see Table I). The prefactors of one-half cure the double counting of pairs in Eq. (17).

The model space $\mathfrak{M}$ basis states are products of ground state doublet states $|1_I\rangle$ and $|2_I\rangle$ over all lattice sites I while excited crystal field states are denoted $|W_I\rangle$ for $W=3,\ldots,13$ on each site I. The state $|P\rangle$ in Eq. (8) is a direct product of crystal field states on different sites with the condition that at least one of the states in $|P\rangle$ lies outside the ground state crystal field doublet; in other words, at least one Tb^{3+} ion must be virtually excited in a state $|n\rangle$ with $n\geq 3$. With this notation in hand, we write the quantum term $H^{(2)}_{\rm eff}\equiv\mathcal{PVRVP}$ as

$$\sum_{I_1,..,I_4}\sum_{\alpha,\beta,\gamma,\delta}\mathcal{P}\left(\mathcal{K}^{\alpha,\beta}_{I_1I_2}J^\alpha_{I_1}J^\beta_{I_2}\right)\mathcal{R}\left(\mathcal{K}^{\gamma,\delta}_{I_3I_4}J^\gamma_{I_3}J^\delta_{I_4}\right)\mathcal{P}.\tag{19}$$

There are a few observations that we can make from Eq. (19) that identify classes of nonvanishing terms. Suppose we choose magnetic sites I_p on the pyrochlore lattice for $p=1,2,3,4$ in Eq.(19). Then, when we evaluate Eq.(19) for all other sites, we obtain unit operators $|1_{I_m}\rangle\langle 1_{I_m}|+|2_{I_m}\rangle\langle 2_{I_m}|$ for all sites I_m with $m\neq 1,2,3,4$. This follows because the resolvent operator $\mathcal{R}$ and projection operators $\mathcal{P}$ are diagonal on each site. In the following, we do not write out all these unit operators explicitly. A second observation is that when we consider a term with magnetic sites I_p ($p=1,2,3,4$) all different, we find that such a term vanishes. The reason for this is that the resolvent and angular momentum operators are sandwiched by projectors into the model space. That way, a virtual excitation induced, for example, by J_{I_3} in the $\mathcal{K}_{I_3I_4}$ bilinear operator must be "de-excited" by an angular momentum operator in the other bilinear operator $\mathcal{K}_{I_1I_2}$, (with $I_1=I_3$, for example). If all I_p are different there can be no virtual excitations and, because the resolvent operator is orthogonal to the model space states, such terms must vanish.

Having found those terms that must always vanish, we now divide all the potentially nonvanishing terms into three classes that we shall analyze in turn in the next three subsections.

CASE A The first class of terms has two groups (I_1,I_2) and (I_3,I_4) of sites, with exactly one site in the first group in common with a site in the second group. In this case, the ion on the common site must be virtually excited and de-excited, and the other two ions remain in their ground doublets. This is because the resolvent operator demands that there be some virtual excitations and that the projectors require that any virtual excitation must be de-excited. So, only when two angular momentum operators (one in each V operator of $\mathcal{PVRVP}$) belong to a given site can that site be virtually excited.

CASE B This class of terms has identical pairs (I_1,I_2) and (I_3,I_4) regardless of label ordering, but with only *one single* ion (I_1 or I_2) that is virtually excited.

CASE C Finally, we shall consider the case where (I_1,I_2) and (I_3,I_4) are identical pairs and where *both* ions are virtually excited.

The virtual excitations belonging to each of these three cases are illustrated in Fig. 5.

It will be convenient, while considering the possibilities enumerated above, to make use of the following explicit

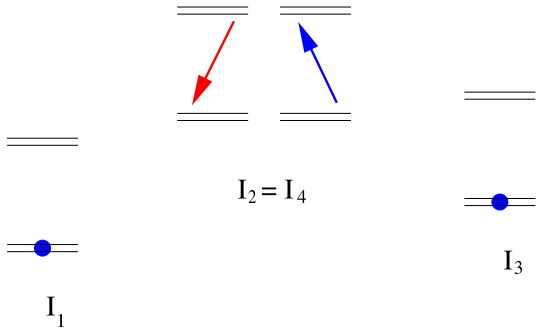

(a) An example of Case A with $I_2 = I_4$ and $I_1 \neq I_3$. Only the ion on site I_2 is virtually excited. The two pairs of sites I_1, I_2 and I_2, I_3 are not restricted to be nearest neighbors because the bare Hamiltonian has long-ranged dipole-dipole interactions.

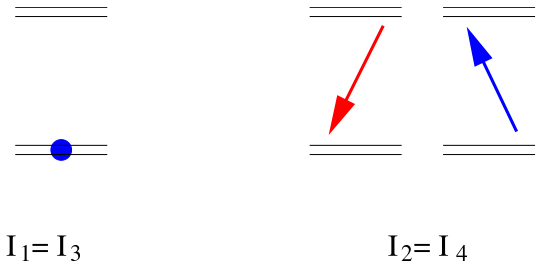

(b) Case B with $I_1 = I_3$ and $I_2 = I_4$ with virtual excitations only on site I_2. There is no virtual excitation on site I_1. I_1 and I_2 need not be nearest neighbors because $\mathcal{K}$ includes an interaction between dipole moments.

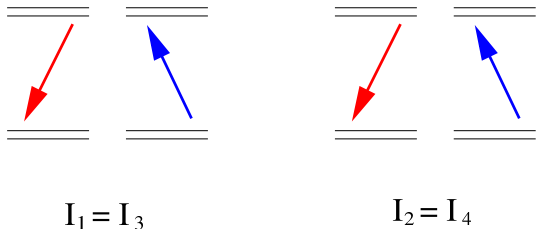

(c) Case C with $I_1 = I_3$ and $I_2 = I_4$. Ions on both sites are virtually excited. Similarly to Cases A and B, I_1 and I_2 need not be nearest neighbors.

FIG. 5: (color online). Figure illustrating the virtual excitations distinguishing three classes of terms in the effective Hamiltonian which are enumerated and described in the main text. The arrows show virtual excitations and de-excitations within the lowest-lying pair of crystal field doublets belonging to the ion on the labeled site. Sites with a blue circle over the ground state doublet indicate that the ion on that site remains in its original state within the ground state crystal field doublet.

decomposition of the quantum term $H_{\rm eff}^{(2)}$:

$$\begin{aligned}\mathcal{P}V\mathcal{R}V\mathcal{P} &= \mathcal{P}H_{\rm ex}\mathcal{R}H_{\rm ex}\mathcal{P} + (\mathcal{P}H_{\rm ex}\mathcal{R}H_{\rm dd}\mathcal{P} \\ &\quad + \mathcal{P}H_{\rm dd}\mathcal{R}H_{\rm ex}\mathcal{P}) + \mathcal{P}H_{\rm dd}\mathcal{R}H_{\rm dd}\mathcal{P}. \quad (20)\end{aligned}$$

We refer to $\mathcal{P}H_{\rm ex}\mathcal{R}H_{\rm ex}\mathcal{P}$ as the exchange-exchange part, $(\mathcal{P}H_{\rm ex}\mathcal{R}H_{\rm dd}\mathcal{P} + \mathcal{P}H_{\rm dd}\mathcal{R}H_{\rm ex}\mathcal{P})$ as the exchange-dipole part and $\mathcal{P}H_{\rm dd}\mathcal{R}H_{\rm dd}\mathcal{P}$ as the dipole-dipole part.

B. Case A

We will show that the situation in Case A described above leads to (i) effective Hamiltonian bilinear interactions between the local z components of the spins and also to (ii) three-body interactions of the form $\tilde{\sigma}^z_{I_1}\tilde{\sigma}^\alpha_{I_2}\tilde{\sigma}^z_{I_3}$ where $\alpha = x$ or y, but not z.

We write the bilinear operator on the left-hand-side of Eq. (19) as $\tilde{\mathcal{K}}^{\alpha,\beta}_{I_1I_2}\widetilde{J}^\alpha_{I_1}\widetilde{J}^\beta_{I_2}$ and the other bilinear as $\tilde{\mathcal{K}}^{\alpha,\beta}_{I_2I_3}\widetilde{J}^\alpha_{I_2}\widetilde{J}^\beta_{I_3}$ with $I_1 \neq I_3$ ($I_2 = I_4$, see Fig. 5(a)) with all angular momentum components referred to the local coordinate system. As we discussed above, the contribution of all the other sites gives identity operators for each site. Omitting these unit operators, we are left with

$$\begin{aligned}&\sum_{\alpha,\beta,\rho,\sigma}\sum_{m_p}\sum_{W}\mathcal{P}(m_1,m_2,m_3)\tilde{K}^{\alpha\beta}_{I_1I_2}\widetilde{J}^\alpha_{I_1}\widetilde{J}^\beta_{I_2} \\ &\quad\times\frac{|m_{4,I_1},W_{I_2},m_{3,I_3}\rangle\langle m_{4,I_1},W_{I_2},m_{3,I_3}|}{E_0-E_W} \\ &\quad\times\tilde{K}^{\rho\sigma}_{I_2I_3}\widetilde{J}^\rho_{I_2}\widetilde{J}^\sigma_{I_3}\mathcal{P}(m_4,m_5,m_6) \quad (21)\end{aligned}$$

with

$$\begin{aligned}\mathcal{P}(m_1,m_2,m_3) &\equiv |m_{1,I_1},m_{2,I_2},m_{3,I_3}\rangle\langle m_{1,I_1},m_{2,I_2},m_{3,I_3}| \\ \mathcal{P}(m_4,m_5,m_6) &\equiv |m_{4,I_1},m_{5,I_2},m_{6,I_3}\rangle\langle m_{4,I_1},m_{5,I_2},m_{6,I_3}|. \quad (22)\end{aligned}$$

E_W is the energy of an excited crystal field state on a single ion. Here, the angular momentum components are expressed in their respective local coordinate systems with local **z** axes given in Table I, the rotation matrices having been absorbed implicitly into $\tilde{K}^{\alpha\beta}_{I_1I_2}$. The integers m_p run over 1 and 2 with the states lying within $\mathfrak{M}_I$ on their respective sites. We factor out the part for site I_1: $\sum_{m_1,m_4}|m_1\rangle\langle m_1|\widetilde{J}^\sigma_{I_1}|m_4\rangle\langle m_4|$. Recalling the property, Eq. (4) and the mapping in Eq. (11), we obtain $\langle\widetilde{J}^z\rangle\tilde{\sigma}^z_{I_1}$. We reach the same result for the sum over states m_3 and m_6 on site I_3. Equation (21) then simplifies to

$$\begin{aligned}&\sum_{\beta,\rho}\tilde{K}^{z\beta}_{I_1I_2}\tilde{K}^{\rho z}_{I_2I_3}\langle\widetilde{J}^z\rangle^2\tilde{\sigma}^z_{I_1}\tilde{\sigma}^z_{I_3} \\ &\times\left(\sum_{m_2,m_5}\sum_{W}|m_2\rangle\langle m_5|\frac{\langle m_2|\widetilde{J}^\beta_{I_2}|W\rangle\langle W|\widetilde{J}^\rho_{I_2}|m_5\rangle}{E_0-E_W}\right) \quad (23)\end{aligned}$$

in the local coordinate system where we have dropped the I_2 site labels from the state vectors enclosed by brackets. After summing over the excited states $|W\rangle$, and rendering the sum of operators in terms of Pauli matrices, we find an Ising interaction term $\tilde{\sigma}^z_{I_1}\tilde{\sigma}^z_{I_3}$ and three-body operators $\tilde{\sigma}^z_{I_1}\tilde{\sigma}^\alpha_{I_2}\tilde{\sigma}^z_{I_3}$ with $\alpha = x, y$ and $\alpha \neq z$ since, if α were to equal z, the three-body term would violate time reversal invariance. The sum over virtual excited state

and the subsequent rendering in terms of Pauli operators is discussed in some more detail in Appendix B

We have reduced the most general three ion terms in $H^{(2)}_{\rm eff}$ (case A) to interactions between pseudospins one-half but we have not made any assumptions yet about the form of the interactions $\mathcal{K}^{\alpha\beta}_{I_1 I_2}$. In the following, we shall consider the four terms of Eq. (20) in turn within Case A. These terms determine the spatial range of the resulting effective interactions between the pseudospins and are obtained by distinguishing the exchange and dipolar parts of $\tilde{K}$ in Eq. (23).

Exchange-exchange part The exchange-exchange part (referring to the first term of Eq. (20)) − which is nothing more than Eq. (23) for $\tilde{K}$ with $\mathcal{D} = 0$ − is a short-range, but not strictly nearest neighbor, effective interaction. If I_1, I_2 and I_3 all lie on the same tetrahedron in the lattice, then the Ising interaction acts between nearest neighbors and, for given I_1 and I_3, there are two choices for the position of the "mediating ion" I_2 as shown in Fig. 6. The thick lines in this figure join the I_1 and I_3 ions via two different choices for the ion I_2 and generate, together with three-body interactions connecting I_1, I_2 and I_3, a nearest neighbor effective Ising interaction between I_1 and I_3. As we describe in more detail later on, this Ising interaction renormalizes the $\mathcal{J}_{\rm classical}$ exchange, defined in Eq. (15). Within a single tetrahedron, the three-body interactions couple all three pseudospins along each of the paths in Fig. 6. There are two other exchange-exchange pseudospin terms arising from Eq. (23) − those for which the interaction extends further than a single tetrahedron. The ions at the endpoints of the lines on the left-hand-side and right-hand-side of the Fig. 7 are coupled, respectively, by effective Ising-like second nearest neighbor interactions and effective third nearest neighbor Ising exchange. The ions along each line - those at the endpoints and the one at the center of each line - interact also via effective three-body interactions. The dependence of the effective couplings for second and third nearest neighbor Ising interactions, on the bare exchange coupling $\mathcal{J}_{\rm ex}$ is shown in Fig. 8 (the dipole-dipole coupling $\mathcal{D}$ being set equal to zero). The second nearest neighbor effective coupling is antiferromagnetic, and the third nearest neighbor effective coupling is ferromagnetic when the bare exchange coupling is antiferromagnetic ($\mathcal{J}_{\rm ex} > 0$). See Section III B for the convention on the exchange that we use in this paper. We note that there are two distinct types of third nearest neighbors on the pyrochlore lattice (see, for example Fig. 1 of Ref. 72 or Fig. 2 in Ref. 73) and that only one type − those connected by one mediating ion, or two edges, along the lattice − appear in $H^{(2)}_{\rm eff}$. Third nearest neighbours of the other type have sites that are connected via three edges along the lattice (as shown by the dotted line of Fig. 7) and hence couplings between ions on these sites would require two mediating ions to appear in the effective Hamiltonian. But, to the (second) order of perturbation theory that we are considering, there is a maximum of one mediating ion so such couplings do not appear in $H^{(2)}_{\rm eff}$.

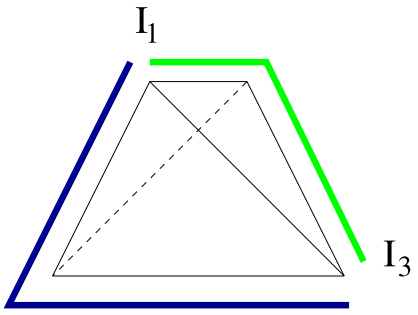

FIG. 6: (color online). In deriving $H^{(2)}_{\rm eff} = \mathcal{P}V\mathcal{R}V\mathcal{P}$, where V is a sum of bilinear interactions, we consider a single pairwise interaction in the right-hand interaction V on sites I_2 and I_3 and a pairwise interaction in the left-hand V between I_1 and I_2. This choice of terms in $H^{(2)}_{\rm eff}$ is referred to as Case A in the main text. Because $I_1 \neq I_3$, and because the operators on these sites are sandwiched between $\mathbf{P}$ projectors, the only virtually excited site is I_2 while the other two sites remain in their (noninteracting) crystal field ground state. As we show in Appendix B, one obtains effective $\tilde{\sigma}^z$ operators on site I_1 and I_3. There are two possibilities for the effective operator on site I_2 after calculation: it could be a unit operator leaving an Ising coupling between sites I_1 and I_3, or it could give rise to a transverse operator $\tilde{\sigma}^x_{I_2}$ or $\tilde{\sigma}^y_{I_2}$, generating an effective three-body term connecting sites I_1, I_2 and I_3. The figure shows a single tetrahedron in a pyrochlore lattice with the two ways of joining sites I_1 and I_3. The total effective Ising exchange for this Case A between ions I_1 and I_3, $J^{zz}_{I_1 I_2}$ is the sum of the Ising exchange terms corresponding to each path in the figure.

Having discussed the exchange-exchange part, we switch on the dipolar interaction. In doing so, the interactions become anisotropic even in the bare Hamiltonian. Nevertheless, in Case A, the types of couplings that arise in the presence of the dipolar coupling are the same as those arising in the exchange-exchange case, the only difference being in the range over which the couplings act.

Exchange-dipole part The exchange-dipole part of the Class A interactions consists of those terms in Eq. (23) with $\mathcal{D}_{\rm ex} = 0$ between, say I_1 and I_2 and $\mathcal{J}_{\rm ex} = 0$ between I_2 and I_3. There are then long-range Ising-like interactions between I_1 and I_3 although the exchange Hamiltonian constrains two sites, I_1 and I_2, in this case, to be nearest neighbors. The bare microscopic dipole interaction acts between sites I_2 and I_3 and decays as $|\mathbf{R}_{I_2 I_3}|^{-3}$. Overall the Case B effective interactions decay as $|\mathbf{R}_{I_1 I_3}|^{-3}$ at long distances just as the bare dipole interactions do on their own. The same is true, by symmetry, of the Class A interactions belonging to the dipole-exchange term in Eq. (20). There are also three-body interactions originating from the exchange-dipole and dipole-exchange parts of Eq. (20) where two of the spins operators must lie on nearest neighbor sites.

Dipole-dipole part Finally, the terms in Class A belonging to the dipole-dipole term of Eq. (20) ($\mathcal{J}_{\rm ex} = 0$

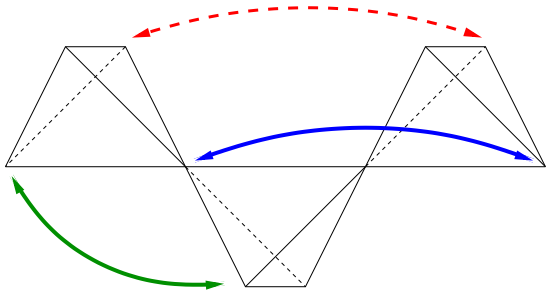

FIG. 7: (color online). Part of a chain of tetrahedra in a pyrochlore lattice. For case A (with only exchange interactions in the bare Hamiltonian), the quantum part, $H_{\rm eff}^{(2)} = \mathcal{P}V\mathcal{R}V\mathcal{P}$, of the effective Hamiltonian has nonvanishing couplings for interactions between the sites connected by the thick lines. The (green) curve on the left-hand-side indicates that Ising exchange acts between second nearest neighbors. The (blue) curve on the right-hand-side indicates that those third nearest neighbors lying along chains of sites are coupled by Ising exchange. The red dashed curve indicates a second type of third nearest neighbor for which no effective coupling is generated as explained in the main text. Three-body interactions also arise that couple all three ions along each of the paths joined in the figure. These further neighbor couplings receive a further contribution when the dipolar coupling is switched on. Also, in the presence of the dipolar interaction, there are off-diagonal effective couplings of the form $J^{\mu\nu}_{I_1I_2}\tilde{\sigma}^{\mu}_{I_1}\tilde{\sigma}^{\nu}_{I_2}$ with $\mu \neq z$, $\nu \neq z$ in addition to an Ising coupling that renormalizes the classical (Ising, first order) DSIM $\mathcal{P}V\mathcal{P}$ term.

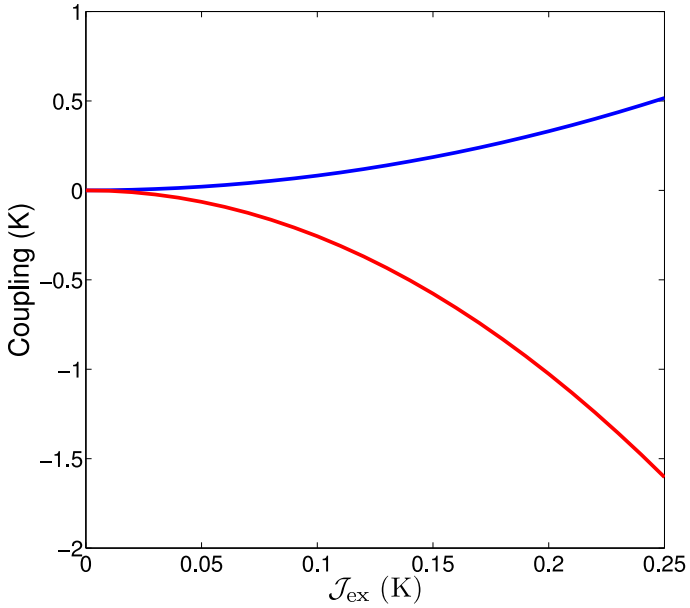

FIG. 8: (color online). Further neighbor Ising interactions generated by quantum fluctuations when $\mathcal{D} = 0$. The upper curve is the second nearest neighbor Ising coupling (between spins with sublattice labels 1 and 3). It is antiferromagnetic in nature. The lower curve is the ferromagnetic third nearest neighbor interaction (between two spins with sublattice label 1 − see straight right-hand blue line in Fig. 7). When $\mathcal{D} \neq 0$, these couplings are renormalized by other contributions from Class A and Class C terms. Since couplings are referred to operators in the local coordinate system, they contain geometrical factors from the rotation matrices (see Sections II A and III B).

in Eq. (23)) have a range that is a product of two dipole interactions so the overall two-body interaction between sites I_1 and I_3 decays as a function of I_2 as $|\mathbf{R}_{I_1I_2}|^{-3}|\mathbf{R}_{I_2I_3}|^{-3}$ before summing over.

In summary, we have learned in this section, in the discussion following Eq. (20), and in Appendix B, that the effective pseudospin operator on the "connecting site" I_2 involved in the virtual excitation process can be a unit operator so that the resulting nontrivial effective interaction is a bilinear of Ising pseudospin operators between I_1 and I_3. In this circumstance, there are contributions to this interaction for I_2 positions at arbitrarily large distances from I_1 and I_3. Together with two body Ising interactions, there are also three spin long-range interactions in this group of terms following from the argument given above. There are no constraints on the positions of the coupled sites I_1, I_2 and I_3 in the lattice.

C. Case B

Now, referring to Eq. (19), we impose the constraint $I_3 = I_1$ and $I_4 = I_2$ and, without loss of generality, suppose that only the ion on site I_2 is virtually excited (see Fig. 5(b)). After computing Eq. (19) with the aforementioned constraint, we obtain a result that is proportional to the unit operator. That is, this case gives rise to a constant shift in energy. As a first step, we write out Eq. (17) with the unit operators on all sites but I_1 and I_2 factored out:

$$\sum_{\alpha,\beta,\rho,\sigma}\sum_{m_p}\sum_{W}\mathcal{P}(m_1,m_2)\tilde{K}^{\alpha\beta}_{I_1I_2}\widetilde{J}^{\alpha}_{I_1}\widetilde{J}^{\beta}_{I_2} \times \frac{|m_3,W\rangle\langle m_3,W|}{E_0-E_W}\tilde{K}^{\rho\sigma}_{I_1I_2}\widetilde{J}^{\rho}_{I_1}\widetilde{J}^{\sigma}_{I_2}\mathcal{P}(m_4,m_5), \quad (24)$$

where the notation $\mathcal{P}(m_1,m_2)$ stands for operator $|m_{1,I_1},m_{2,I_2}\rangle\langle m_{1,I_1},m_{2,I_2}|$. Because only the ion on site I_2 is virtually excited, the operator $\widetilde{J}^{\alpha}_{I_1}$ acts entirely on states within $\mathfrak{M}_{I_1}$ so, referring to the matrix elements in Eq. (4) we obtain, for ion I_1,

$$|1_{I_1}\rangle\langle 1_{I_1}|\langle 1_{I_1}|\widetilde{J}^{z}_{I_1}|1_{I_1}\rangle^2 + |2_{I_1}\rangle\langle 2_{I_1}|\langle 2_{I_1}|\widetilde{J}^{z}_{I_1}|2_{I_1}\rangle^2 = \langle\widetilde{J}^{z}_{I_1}\rangle^2\mathbb{I}_{I_1} \quad (25)$$

− the unit operator acting on I_1, which we can omit in the following. When the sum is performed over excited crystal field states on ion I_2, the resulting operators map to the unit operator $\mathbb{I}_{I_2}$ and Pauli matrices $\tilde{\sigma}^{x}_{I_2}$ and $\tilde{\sigma}^{y}_{I_2}$ − all the resulting operators being consistent with time reversal. This calculation is performed along the lines described in Appendix B.

It would thus seem that, together with the constant energy shift, there are effective nontrivial single-site transverse field operators in the effective Hamiltonian of the form $\tilde{\sigma}^x$ and $\tilde{\sigma}^y$. However, these effective transverse field terms cancel on any given lattice site when one sums the contributions to these single-site operators coming from the bare microscopic pairwise interactions in V. Without going into the details of the sum over different contributions to site I_2 we see that there must be such a cancellation because neither the original model nor the effective Hamiltonian formalism distinguishes particular directions (as opposed to particular axes) on individual sites. When the Tb^{3+} ions are randomly diluted with nonmagnetic ions, as in $(Tb_pY_{1-p})_2Ti_2O_7$,[74] there is no longer perfect cancellation of the effective single site operators. These effective fields have the effect of splitting the degenerate $|1\rangle$, $|2\rangle$ doublet on each ion for which the cancellation does not occur. So, in fact, the low energy effective theory of the diluted compound $(Tb_pY_{1-p})_2Ti_2O_7$ would be somewhat different than that of the pure $Tb_2Ti_2O_7$ by admitting effective random transverse fields. The possible generation of effective random transverse fields generated by dilution in $(Tb_pY_{1-p})_2Ti_2O_7$ had previously been proposed in Ref. 75. In the remainder of the article, we shall assume that the magnetic ions are not diluted.

D. Case C

The class of terms where the two ions I_1 and I_2 are both virtually excited (see Fig. 5(c)) is the most complicated of the three cases A,B and C in the sense that all two body terms consistent with time reversal and the lattice symmetries can and do arise. Because the dipolar coupling is nonzero, long range effective interactions appear in $H_{\rm eff}$. The calculation of the types of terms and their couplings in Case C is most easily accomplished by the projection method given in Appendix B. In this section then, we give only the results of this calculation − the means of calculation having been outlined in the discussion of Section IV B and in Appendix B. As with the terms in Case B, the net single-site "fields", $\tilde{\sigma}^x$ and $\tilde{\sigma}^y$ cancel, leaving the Ising interaction $\tilde{\sigma}^z_{I_1}\tilde{\sigma}^z_{I_2}$, and the transverse exchange interactions $\tilde{\sigma}^\alpha_{I_1}\tilde{\sigma}^\beta_{I_2}$ where each of α and β can be x and y.

We make the observation here, that is discussed in more detail in Appendix B, that the transverse exchange interactions can appear in the effective Hamiltonian from VCFEs involving only the ground state doublet and first excited states because there are nonvanishing $\tilde{J}^x$, $\tilde{J}^y$ and $\tilde{J}^z$ matrix elements between these states. Hence, the appearance of these effective transverse exchange interactions in $H^{(2)}_{\rm eff}$ is strongly tied to the specific form of the $Tb_2Ti_2O_7$ single ion crystal field wavefunctions.

Because the bare exchange interaction vanishes if I_1 and I_2 are not nearest neighbors, even if one of the bilinear interactions in Eq. (20) is a dipole-dipole interaction, the cutoff coming from the bare exchange ensures vanishing of the effective interaction beyond nearest neighbor for Case C. This means that the only interactions in Case C extending beyond nearest neighbors come from the dipole-dipole part of Eq. (20) and, because there are only two ions involved in Case C (see Fig. 5(c)), the interaction falls off as the square of the dipole-dipole interaction: $1/|\mathbf{R}_{I_1I_2}|^6$.

E. Treatment of the dipole-dipole interactions

In Section V, the semiclassical ground states of the effective Hamiltonian are computed first on a single tetrahedron (Section V B), then on a periodic cubic unit cell (Section V D). In the former case, the bare dipole-dipole interaction, $H_{\rm dd}$, is truncated beyond nearest neighbors. In the latter case, one should not truncate the long-range dipole-dipole interaction. This problem has been approached in two ways. The first way is to derive the effective interactions on a finite but large lattice. Then, to obtain the interaction between sublattices a and b on a periodic unit cell with sixteen sublattices, the interactions between sublattice a and all the periodic images of b on the large lattice are summed up. A second way to treat the long-range dipole is to compute the bare microscopic interactions on a periodic cubic unit cell by an Ewald summation[54,76] and then to derive the effective Hamiltonian respecting the periodicity. The first approach was used in Ref. 77. Here we use the latter.

F. Summary

We have now worked out the different types of effective interactions that arise in the Hamiltonian $H_{\rm eff}$ obtained from the model of Section II A for $Tb_2Ti_2O_7$ to lowest order in the virtual crystal field excitations (VCFEs). Before describing previously published results obtained from the effective Hamiltonian when considering a single (isolated) tetrahedron, we briefly summarize here the results of Sections III and IV.

The effective Hamiltonian for $Tb_2Ti_2O_7$ has been derived to order $(\langle V\rangle/\Delta)$ which includes a classical part and also interactions coming from VCFEs to lowest order. The classical part of the effective Hamiltonian is given by $\mathcal{P}V\mathcal{P}$ and is nothing other than the dipolar spin ice model (DSIM) with Ising exchange $\mathcal{J}_{\rm classical}$ and dipole-dipole couplings that merely differ from those of the microscopic model (Section II A) by a constant factor related to the expectation value of the bare angular momentum in the crystal field ground states; $\mathcal{J}_{\rm classical} = \mathcal{J}_{\rm ex}\langle\tilde{J}^z\rangle^2$.

The effective Hamiltonian $H_{\rm eff}$ is expressed in terms of spin one-half operators which have different time reversal properties (Eq. (14)) compared to true angular momentum operators. A large number of different pseudospin interactions appear in the quantum term $H^{(2)}_{\rm eff}$. These are constrained to be invariant under time reversal and

to respect lattice symmetries. If we switch off the dipole-dipole interaction temporarily ($\mathcal{D} = 0$), we find nearest neighbor Ising interactions which renormalize those from the classical term and, also, transverse terms of the form $\tilde{\sigma}^{\alpha}_{I_1}\tilde{\sigma}^{\beta}_{I_2}$ where α, β can be components x or y. Effective interactions beyond nearest neighbor are Ising exchange interactions between second nearest neighbors and one out of the two distinct types of third nearest neighbors on the pyrochlore lattice (see Fig. 7). Finally, three-body interactions of the form $J^{zxz}\tilde{\sigma}^z\tilde{\sigma}^x\tilde{\sigma}^z$ are also generated. When dipole-dipole interactions are restored, ($\mathcal{D} \neq 0$), $H_{\rm eff}$ acquires two new types of effective interaction.

1. New short-range interactions acting between nearest neighbors and beyond, decaying as $1/|\mathbf{R}|^6$.

2. Long range interactions decaying as $1/|\mathbf{R}|^3$.

Both contributions, arising when the dipole-dipole interactions are switched on, further renormalize the effective nearest neighbor Ising coupling and contribute to the transverse effective couplings.

For later reference we write the nearest neighbor effective couplings between ions on sites I_1 and I_2 as

$$J^{zz}_{I_1I_2}\tilde{\sigma}^z_{I_1}\tilde{\sigma}^z_{I_2} + J^{\alpha\beta}_{I_1I_2}\tilde{\sigma}^{\alpha}_{I_1}\tilde{\sigma}^{\beta}_{I_2}. \tag{26}$$

where α and β can each equal x and y.

Now we consider the relative magnitude of some different effective couplings on a lattice which will be of use in later sections when we interpret our ground state phase diagrams. Fig. 9 shows three different effective Hamiltonian couplings as a function of the bare exchange coupling $\mathcal{J}_{\rm ex}$ when the dipole-dipole coupling $\mathcal{D}$ is fixed at the value for $Tb_2Ti_2O_7$; $\mathcal{D} = 0.0315$ K. The three couplings are for nearest neighbor interactions $J^{zz}\tilde{\sigma}^z\tilde{\sigma}^z$ and $J^{xx}\tilde{\sigma}^x\tilde{\sigma}^x$ and the three-body interaction $J^{zxz}\tilde{\sigma}^z\tilde{\sigma}^x\tilde{\sigma}^z$, all expressed in the local coordinate system. The transverse bilinear couplings are averaged over the bonds on a single tetrahedron to give an idea of the scale of the interactions while the three-body coupling is plotted for bonds connecting sublattices 1, 2 and 3 on a single tetrahedron (see Table I) which is representative of the scale of these interactions. Looking at these nearest neighbor couplings, we see that the Ising interaction changes sign at about $\mathcal{J}_{\rm ex} \approx 0.2$ K. For $\mathcal{J}_{\rm ex} < 0.2$ K, the Ising interaction favors ice-like order and, for $\mathcal{J}_{\rm ex} > 0.2$ K, it favors all-in/all-out ordering (see Fig. 14(a)). The Ising coupling J^{zz} is the largest coupling over most of the range of $\mathcal{J}_{\rm ex} \lesssim 0.2$ K, followed by transverse couplings, for instance J^{xx}, and then the three-body interaction J^{zxz}. For $\mathcal{J}_{\rm ex} \gtrsim 0.2$ K, the Ising and transverse couplings are of similar magnitude. This is therefore a direct microscopic derivation showing the restoration of effective pseudospin isotropy that is discussed in Refs. 27 and 54.

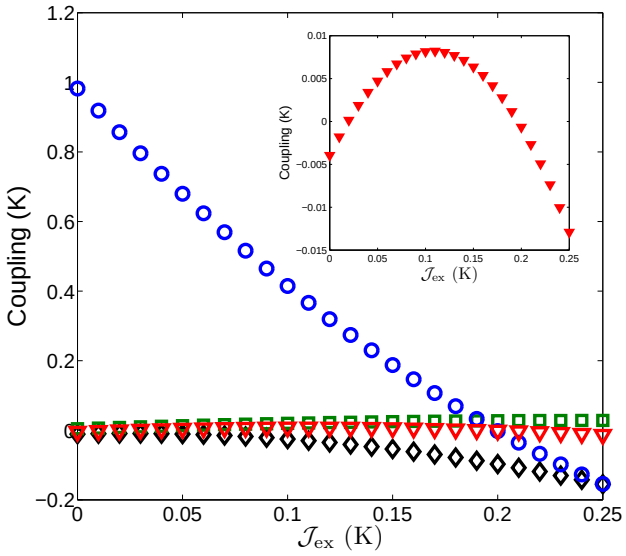

FIG. 9: (color online). Plot showing the variation of various couplings in the effective Hamiltonian on a lattice, as a function of the bare exchange coupling $\mathcal{J}_{\rm ex}$. The bare Hamiltonian has long-range dipole-dipole interactions. We plot bilinear Ising J^{zz}, transverse J^{xx} and J^{yy} couplings (Eq. (26)) between nearest neighbor sublattices 1 and 2 and a three-body coupling J^{zxz} connecting sublattices 1, 2 and 3. The difference between the J^{xx} and J^{yy} couplings is due to the choice of local x and y axes. All couplings refer to pseudospin couplings in the local coordinate system. The Ising coupling changes sign at about $\mathcal{J}_{\rm ex} \sim 0.2$ K implying a cross-over from ice-like order to AIAO order in the absence of other interactions. For $\mathcal{J}_{\rm ex} \gtrsim 0.2$ K, the Ising and transverse terms are of similar magnitude. The three-body coupling is the weakest of the three interactions; its variation is shown in the inset.

G. Relation with previous results

In Section III and so far in Section IV, we have presented a derivation of an effective Hamiltonian for $Tb_2Ti_2O_7$ to lowest order in the quantum corrections to the DSIM − that is, to order $\langle V\rangle/\Delta$. If this model is to prove useful, it is important to ensure that $\langle V\rangle/\Delta$ is not so large that higher order terms contribute significantly to the low energy physics of $Tb_2Ti_2O_7$. To test the assertion that higher order terms (those of order $(\langle V\rangle/\Delta)^n$ for $n \geq 2$) are not required, a direct comparison was made in Ref. 33 with a microscopic model. This microscopic model is the one presented in Section II A, but with the microscopic exchange and dipolar interactions restricted to spins on a single tetrahedron and with the crystal field spectrum cut off beyond the four lowest energy states. More precisely, instead of diagonalizing the full model $H_{\rm cf} + V$, the single ion crystal field Hamiltonian is diagonalized to obtain states $|n\rangle$ and corresponding energies E_n, whereupon all but the lowest two doublets are neglected leaving, as the new (truncated,"tr") crystal field

Hamiltonian,

$$H_{\rm cf,tr} = \sum_{I_p} E_0(|1_{I_p}\rangle\langle 1_{I_p}| + |2_{I_p}\rangle\langle 2_{I_p}|) + (E_0+\Delta)(|3_{I_p}\rangle\langle 3_{I_p}| + |4_{I_p}\rangle\langle 4_{I_p}|). \quad (27)$$

This model should be a good approximation for sufficiently weak interactions given that, when interactions are switched on, the excited crystal field levels admix into the ground state doublet with the first excited levels having the greatest contribution to the new ground state out of all the excited levels.[78] Including interactions on a single tetrahedron within the basis of four single ion states on each site, the model was diagonalized exactly for a range of bare exchange couplings $\mathcal{J}_{\rm ex}$. For comparison, the effective Hamiltonian was derived on a single tetrahedron and diagonalized computationally to obtain its spectrum. One comparison that has been made from these spectra involves looking at the variation in the ground state degeneracy as a function of the bare exchange coupling, $\mathcal{J}_{\rm ex}$, and the crystal field gap as shown in Fig. 3. As the bare exchange coupling $\mathcal{J}_{\rm ex}$ and the gap Δ are varied, with $\mathcal{D}$ fixed to $\mathcal{D} = 0.0315$ K, there is a phase boundary between a region with a singlet ground state and a region with a doublet ground state. The boundary between these regions is the same for both the effective Hamiltonian and the model with a truncated crystal field spectrum when the gap Δ is infinite. The boundaries move apart as Δ decreases. However, the difference between the two phase boundaries remains relatively fairly small even when the gap is about 18 K, as for $Tb_2Ti_2O_7$; $\mathcal{J}_{\rm ex}(\Delta = 18{\rm K})$ for the phase boundaries agree to within ten percent. Perhaps most importantly, both calculations agree that, as the gap decreases, the region of parameter space over which the singlet occurs becomes larger. For the parameters estimated for $Tb_2Ti_2O_7$,[30,43] the single tetrahedron ground state is a singlet. The ground state for the microscopic model, for the $Tb_2Ti_2O_7$ parameters, is mainly a superposition of two-in/two-out states. For this reason, this state has been called a *quantum spin ice*.[33,67]

That the singlet ground state of the microscopic model shows spin ice-like correlations can be understood from the effective Hamiltonian. It is, at first sight, a peculiar result given the classical DSIM phase diagram described in Section III for which the $Tb_2Ti_2O_7$ parameters lie in the AIAO phase. The explanation for this behavior lies in the fact that, as the gap Δ is lowered, for fixed $Tb_2Ti_2O_7$ bare parameters, the nearest neighbor Ising exchange coupling J^{zz} (Eq. (26)) is renormalized by Ising terms coming from the quantum fluctuations $H^{(2)}_{\rm eff} \equiv \mathcal{PVRVP}$ (see Section IV). The variation of Ising exchange J^{zz} due to VCFEs as a function of the bare exchange is shown in Fig. 10 when the dipole-dipole coupling $\mathcal{D} = 0$. The straight line is the part from the classical term $\mathcal{PVP}$ for which the renormalized (Ising) exchange is $\mathcal{J}_{\rm classical} = \mathcal{J}_{\rm ex}\langle\widetilde{J}^z\rangle$ (where $\langle\widetilde{J}^z\rangle$ is given in Eq. (4) and this formula in derived in Section III). The Ising exchange J^{zz} from the quantum fluctuations is antiferromagnetic ($J^{zz} > 0$) so the sum of the classical and quantum Ising couplings is less ferromagnetic (negative) than the J^{zz} without VCFEs. Now consider the effect of including nearest neighbor dipole-dipole coupling. With the dipole-dipole coupling alone ($\mathcal{J}_{\rm ex} = 0$), J^{zz}, is antiferromagnetic ($J^{zz} > 0$), favoring spin ice correlations (see Section III B). Indeed, in the $Dy_2Ti_2O_7$ and $Ho_2Ti_2O_7$ spin ice materials, the exchange contribution to the Ising J^{zz} coupling is ferromagnetic but the dipole-dipole coupling ensures that the net contribution of the bare microscopic couplings to J^{zz} is antiferromagnetic hence frustrating a single tetrahedron and the pyrochlore lattice.[45] In contrast, we see in the lower part of Fig. 10, that the estimated bare exchange coupling in $Tb_2Ti_2O_7$ of $\mathcal{J}_{\rm ex} \sim 0.17$K,[30] places the classical part of the Ising coupling (i.e. the contribution to J^{zz} from $\mathcal{PVP}$) close to zero. But, VCFE corrections lead to an effective antiferromagnetic coupling $J^{zz} > 0$ overall leading to spin ice-like correlations for $Tb_2Ti_2O_7$.

In another development, the truncated model with six crystal states per site on a tetrahedron was found to exhibit a magnetization plateau in a [111] field below 100 mK − further evidence that this model exhibits spin ice-like behavior for more antiferromagnetic bare couplings than one would expect from the DSIM.[67]

In summary, this article is devoted to a derivation of a quantum spin-1/2 model with anisotropic interactions similar to the models used as starting points in Refs. 38 and 39. From this effective Hamiltonian, we establish two things. Firstly, we show that the renormalization of the Ising exchange towards antiferromagnetic exchange ($J^{zz} > 0$) via VCFEs occurs, not only on a single tetrahedron, but also on the full pyrochlore lattice. That is, even if, at the classical level (which ignores exited crystal field levels), $Tb_2Ti_2O_7$ could be described by a non-frustrated [111] pyrochlore Ising model, virtual crystal field excitations can render this system a frustrated spin ice one, with additional transverse fluctuations. This is the main result of this paper. Secondly, in what follows, we study the semiclassical spin correlations that these effective interactions produce on a lattice.

V. SEMICLASSICAL GROUND STATES

A. Convention and Procedure

The effective Hamiltonian that was discussed in detail in the previous sections has a large number of different effective interactions arising from virtual crystal field excitations (VCFEs) from the ground state crystal field doublet (see Section IV F). As we have seen, to lowest (first) order in the perturbation expansion in $\langle V\rangle/\Delta$, the effective Hamiltonian is an Ising model. The lowest order quantum corrections to $H_{\rm eff}$ include transverse terms between nearest neighbor spins, three-body interactions, and anisotropic interactions extending be-

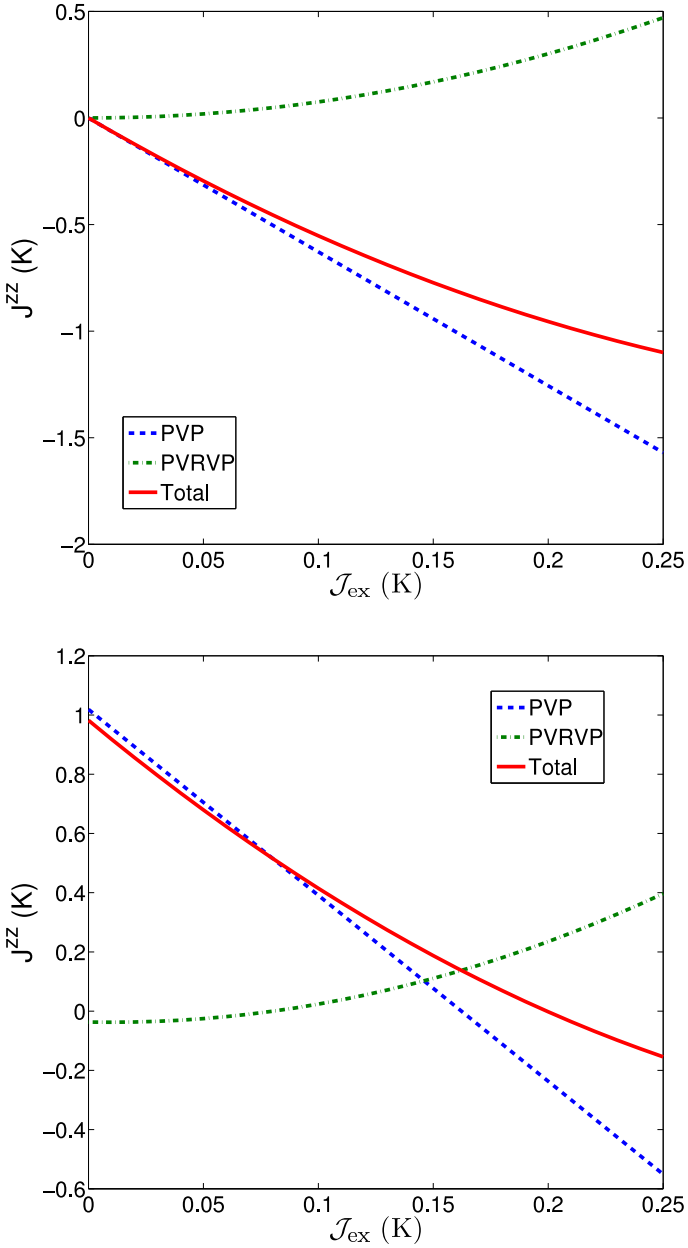

(b) Isotropic exchange and long-ranged dipole-dipole interaction.

FIG. 10: (color online). Plot showing how the nearest neighbor Ising exchange coupling J^{zz} on a lattice (Eq. (26)) is renormalized by the quantum terms of the effective Hamiltonian. The horizontal axis is the bare exchange coupling $\mathcal{J}_{ex}$. The top figure is for the Ising coupling when the dipole-dipole coupling is set equal to zero and the bottom figure includes the dipole-dipole coupling of magnetic ions in $Tb_2Ti_2O_7$: $\mathcal{D} = 0.0315$ K. In both figures, the dashed line is the coupling that appears to lowest order $\mathcal{P}H\mathcal{P}$ in $H_{\rm eff}$ for a pair of neighboring sites. The dot-dash line is the correction obtained from the quantum term $H^{(2)}_{\rm eff}$ and the solid line is the sum of the two contributions to the Ising exchange. A positive J^{zz}, in the absence of other interactions, favors spin ice configurations on each tetrahedron and a negative sign implies AIAO configurations.

yond nearest neighbors. To gain some understanding of the effect of the extra terms generated by VCFEs on the physics of this system, it is useful to consider a semiclassical spin model with the same interactions as in the effective quantum Hamiltonian.

To obtain the required semiclassical model, we first observe that the effective quantum Hamiltonian should be written in terms of pseudospins one-half. That is, the elementary quantum spins take the form $\hat{S}^\alpha = (1/2)\sigma^\alpha$ and the quantum Hamiltonian couplings derived in the previous section are rescaled by a factor of four for the bilinear interactions and by a factor of eight for the three-body interactions. This model is the most suitable model to consider from the point of view of a large spin S expansion. Once the quantum Hamiltonian is written in terms of spins $\hat{S}^\alpha$, we take these quantum spins into classical spins which are vectors of fixed length $S = 1/2$ with components parameterized by spherical polar angles.

To find the ground states of the semiclassical model, we start with a randomly chosen initial spin configuration on a finite lattice and compute its energy. We then make a small random rotation of one of the pseudospins and accept this configuration only if the energy of the new configuration is lower than that of the old configurations. This procedure is iterated until it converges, which happens within $O(10^4)$ steps. This zero temperature Monte Carlo may settle into a local rather than a global minimum. To alleviate this problem, we repeat the process for a number of initial states depending on the number of spins treated and look for the minimum energy configuration; this also allows us to capture any ground state degeneracy.

Only a small number of independent spins are treated in this minimization procedure - we find the ground states on a single tetrahedron (four spins) and on a cubic unit cell with periodic boundary conditions (sixteen spins). With this number of spins, we find that only a small number of initial spin configurations $O(10^1)$ is necessary in the iteration scheme to find consistency between the final energies and to capture discrete degeneracy when it arises. However, if there is a continuous degeneracy, (as in the XY phase described below), $O(10^2)$ initial spin configurations are necessary to confirm its existence. On a cubic unit cell, we capture the DSIM ground states with ordering vector $\mathbf{q} = 001$ and $\mathbf{q} = 0$ in the limit of $1/\Delta = 0$. When Δ is finite, VCFEs generate interactions beyond the DSIM interactions which may lead to more complicated (modulated magnetic moment with incommensurate wavevector $\mathbf{q}$) ground states might be eliminated by (an inappropriate choice of) periodic boundary conditions. Whether this is indeed the case for the $H_{\rm eff}$ considered below is an open question for future work. The key problem we address in computing the ground states is to establish whether interactions generated by VCFEs beyond nearest neighbor do favor spin ice correlations over a wider range of $\mathcal{J}_{ex}$ than is observed in the absence of such terms.

B. Ground states of $H_{\rm eff}$ on a single tetrahedron - 4 CF states

The first results that we present are those obtained by minimizing the energy on a single tetrahedron to make a comparison with the results of exact diagonalization of the four crystal field state microscopic quantum model on a single tetrahedron described in Section IV G. The effective Hamiltonian required to make the comparison includes the nearest neighbor interactions and three-body interactions on a single tetrahedron obtained by including only the first excited crystal field doublet in the resolvent (Eq. (8)) when computing the quantum terms, $H_{\rm eff}^{(2)}$. By truncating all the bare interactions to a single tetrahedron, the effective Hamiltonian is derived following Section IV including all possible ways that the mediating ion of Case A in Section IV B can lie on a single tetrahedron. Cases B and C (Sections IV C and IV D) are treated entirely on the single tetrahedron. At first, we present the results when the three-body terms are omitted; we include them later. When three-body terms are omitted and the derived effective interactions are truncated beyond nearest neighbors, the ground states on a single tetrahedron must coincide with those on the full lattice under the assumption that the lattice ground states have $\mathbf{q} = 0$ ordering wavevector. This is because the interactions for a $\mathbf{q} = 0$ lattice configuration are the same as those on a single tetrahedron except for an extra factor of two in the effective couplings on the lattice. This factor of two comes from the fact that pairwise effective interactions couple a spin on one sublattice, a, to two b sublattices ($a \neq b$) whereas, on a tetrahedron, a spin with sublattice label a couples to only one b sublattice spin.

The ground states are shown in Fig. 11. This figure shows the energies computed from the effective Hamiltonian with classical spins on a single tetrahedron for different (imposed) specific spin configurations and for different values of the bare exchange, $\mathcal{J}_{\rm ex}$. The energies of the ground states determined by the minimization procedure outlined above are shown as well.

One finds that as the bare exchange coupling $\mathcal{J}_{\rm ex}$ (for fixed dipole-dipole coupling $\mathcal{D} = 0.0315$ K) becomes more antiferromagnetic (i.e. positive and larger), the two-in/two-out ground state gives way to an all-in/all-out state (Fig. 14). However, unlike the classical model, $\Delta = \infty$, for which only the two-in/two-out and all-in/all-out states appear, there is a $\mathbf{q} = 0$ configuration separating the two-in/two-out state from the all-in/all-out state in which the classical spins lie fully in their local XY planes perpendicular to the local [111] directions.

There is a continuous degeneracy of XY configurations such that the vector sum of the spins is zero as one should expect for sufficiently strong antiferromagnetic exchange. A single spin configuration among the continuous set of XY ground states is illustrated in Fig. 14(b). These ground states belong to the two dimensional irreducible representation of the point group of the tetrahedron O_h (see, Refs. 63 and 79) which includes the discrete ground states of the material $Er_2Ti_2O_7$ (see, for example, Ref. 14). The onset of the XY phase corresponds to a range of values of the bare exchange $\mathcal{J}_{\rm ex}$ where the effective Ising and transverse couplings (shown in Fig. 9) are of similar magnitude such that it is energetically favorable for the spins to lie in the local XY planes.

For the classical DSIM with dipole-dipole interactions truncated beyond nearest neighbor, there is a phase boundary[45] between a spin ice state and an all-in/all-out phase at $\mathcal{J}_{\rm ex} = 5\mathcal{D}$ which is roughly 0.158 K for the $Tb_2Ti_2O_7$ dipolar coupling $\mathcal{D} = 0.0315$ K. Reading from the phase diagram in Fig. 11, the spin ice to XY boundary of the nearest neighbor effective Hamiltonian is at about 0.17 K and the onset of the all-in/all-out (AIAO) phase is at about $\mathcal{J}_{\rm ex} = 0.22$ K for the effective Hamiltonian on a single tetrahedron. A direct comparison of these numbers with the classical model (DSIM) is possible because (i) the phase boundary of the DSIM depends on the ratio of the effective Ising exchange $\mathcal{J}_{\rm classical}$ (Eq. (15)) to the effective dipole couplings $\mathcal{D}_{\rm classical}$ (Eq. (16)) and (ii) the ratio of effective couplings in the classical term $\mathcal{PVP}$ is simply the ratio of bare couplings. That the phase boundary out of the two-in/two-out Ising configuration in the semiclassical effective model appears for more positive $\mathcal{J}_{\rm ex}$ than with the classical term ($\mathcal{PVP}$) alone is because the effective Ising exchange, J^{zz}, in the quantum model receives a contribution from $H_{\rm eff}^{(2)}$ that makes it more antiferromagnetic (J^{zz} becomes more negative) hence making spin ice Ising configuration energetically favorable. We mention also that the effective Ising coupling, J^{zz}, between $\mathcal{J}_{\rm ex} = 0.17$ K and $\mathcal{J}_{\rm ex} = 0.20$ K is antiferromagnetic (positive) whereas $H_{\rm eff}$ calculated solely to $\mathcal{PVP}$ order has ferromagnetic effective Ising exchange (favoring all-in/all-out order) over this range.

When we include the three-body terms on a single tetrahedron, we again find three ground state phases with the same phase boundaries that we found in the two-body case. Whereas the AIAO phase is the same with and without three-body terms, the other two two-body phases are modified by the introduction of three-body couplings. Instead of ground states with spins aligned along the local Ising directions, one finds that the spins are canted away from the [111] directions while retaining the spin ice ordering in the Ising components. The canting (which is shown in Fig. 12 for one of the observed ground states) is such as to preserve the moment of the perfectly Ising spin configuration. The variation in the canting angle is shown in the inset to Fig. 11. Only in the spin ice regime, $\mathcal{J}_{\rm ex} < 0.17$ K, are the ground states affected by a canting away from the Ising directions when three-body interactions are included. The three-body terms do not produce a canting away from the two-body XY and AIAO ground states. Also, with three-body interactions included, the degenerate XY configurations cease to be the lowest energy states in the intermediate region $0.17\ {\rm K} \lesssim \mathcal{J}_{\rm ex} \lesssim 0.22$ K - the continuous degeneracy present without three-body terms is broken.

The transverse (XY) components of the spins in the spin canted state are ordered into six discrete configurations. The transverse component configurations, considered on their own, are a discrete set of configurations belonging to the aforementioned class of XY ground states − they are referred to as ψ_2 states in the literature.[14,63,79] The canting angle is zero in the AIAO phase.

Turning to the ground state energies themselves in the presence of three-body interactions, we first note that the three-body terms make no contribution to the XY and perfectly Ising spin configurations because the three-body terms are of the form $\tilde{\sigma}^z_{I_1}\tilde{\sigma}^\alpha_{I_2}\tilde{\sigma}^z_{I_3}$ with $\alpha = x, y$ which vanishes in these cases. However, the perfectly Ising-like spin ice configurations are not true ground states when three-body terms are present for $\mathcal{J}_{\rm ex} \lesssim 0.27$ K - there is a small canting away from the Ising directions. There is a difference between the two and three-body ground state energies that is small (about 4% at most) arising from the relative sizes of the two and three body couplings illustrated in Fig. 9.

Fig. 9 is useful in interpreting the single tetrahedron ground state diagrams (with or without three-body interactions). In both phase diagrams, the sign of the Ising coupling determines the correlations of the Ising components of the classical spins (which, as we report in Section V D ceases to be true beyond a single tetrahedron), and the relative magnitude of the Ising coupling and other couplings is correlated to the canting of the spins away from the Ising directions − the spins being furthest from the Ising directions when the transverse couplings become comparable to or greater than the Ising coupling.

Now we are in a position to compare the single tetrahedron results for the quantum four crystal field state (ground and first excited doublet) effective Hamiltonian with the classical results. The quantum phase diagram showing the ground state degeneracies is plotted in Fig. 3. Focusing on the $Tb_2Ti_2O_7$ crystal field gap of $1/\Delta = 0.055$ K^{-1}, the boundary between the singlet and doublet states is at about $\mathcal{J}_{\rm ex} = 0.21$ K (with $\mathcal{D} = 0.0315$ K). The phase boundary for the semiclassical ground state derived from the effective Hamiltonian (Fig. 11) is close to this value, at about $\mathcal{J}_{\rm ex} = 0.22$ K. The degeneracies of the semiclassical ground states and the quantum ground states on a single tetrahedron agree for $\mathcal{J}_{\rm ex} > 0.22$ K whereas for $\mathcal{J}_{\rm ex} < 0.22$ K, the singlet quantum ground state appears for the same range of couplings as both the classical six-fold degenerate canted spin ice ground state and the XY phase.

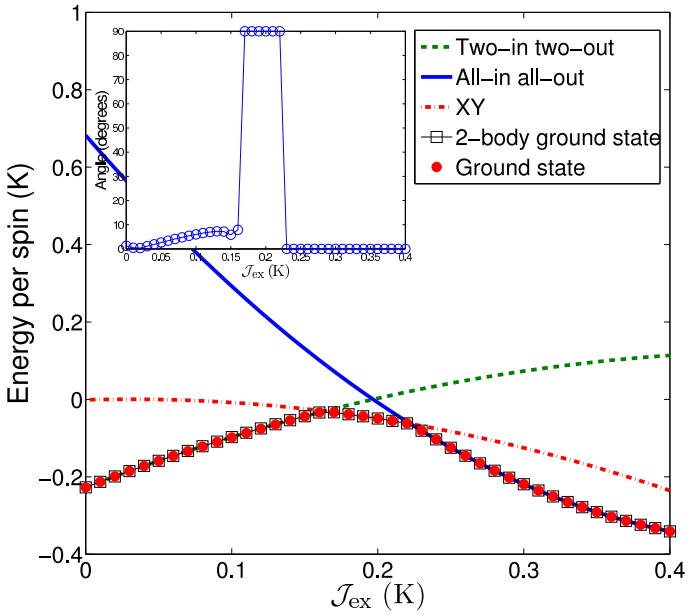

FIG. 11: (color online). Semiclassical ground state energy of the effective Hamiltonian on a single tetrahedron when quantum terms are computed including VCFEs only to the first excited crystal field doublet (i.e. omitting virtual excitations to higher energy crystal field states). In obtaining these results, the bare microscopic exchange, $H_{\rm ex}$, and dipolar interaction, $H_{\rm dd}$, were truncated at the nearest neighbor distance. The resulting effective couplings generated in $H^{(2)}_{\rm eff}$ were also truncated beyond nearest neighbor. The parameters used for this calculation are $\Delta^{-1} = 0.055$ K^{-1}, $\mathcal{D} = 0.0315$ K and $\langle\tilde{J}^z\rangle = 3.0$. Also plotted, are energies of three different imposed spin configurations. The omission of three-body interactions changes the ground state energy by a few percent depending on the canting angle produced by these interactions. The inset shows the angle from the local **z** axes of Table I through which the spins are canted in the ground states of the model - for $\mathcal{J}_{\rm ex} \lesssim 0.17$ K, the canting is due to the three-body interactions and the 90 degree canting angles signal the onset of the local XY ground states which are ground states even without the three-body interactions.

C. Ground states of $H_{\rm eff}$ on a single tetrahedron - 13 CF states

Before leaving the subject of the ground states on a tetrahedron, we compute the ground states on a single tetrahedron with the full crystal field spectrum included in the resolvent operator (rather than considering a truncation of the spectrum to the ground and first excited doublets as we have done in Section V B). In this subsection, the ground states of $H_{\rm eff}$ we present were computed as a function of both $\mathcal{J}_{\rm ex}$ and Δ. Here Δ is an adjustable gap that shifts all the excited crystal field states rigidly with respect to the ground state doublet leaving the wavefunctions identical to those that one would obtain by diagonalizing the $Tb_2Ti_2O_7$ crystal field Hamiltonian. By artificially varying Δ in this way, we can tune the system from a classical spin ice with nearest neighbor dipolar interactions to a model in which VCFEs are significant. The results are shown in Fig. 13. As one would expect based on the limiting case $1/\Delta = 0$ of spin ice and the results discussed in Section V B for $1/\Delta = 0.055$ K^{-1}, the all-in/all-out ground states and the two-in/two-out ground states are separated by a wedge of ordered lo-

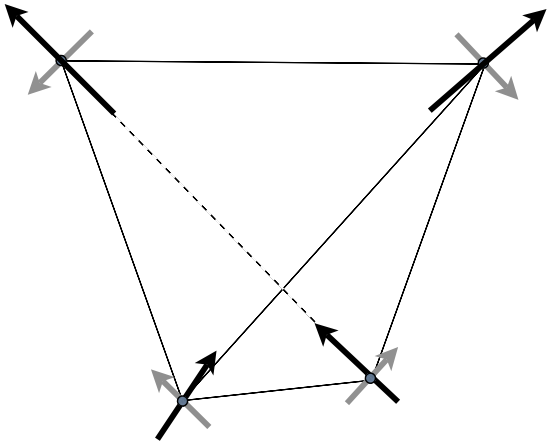

FIG. 12: The semiclassical LRSI_{000} ground state of the effective Hamiltonian represented on a single tetrahedron. The black arrows show the local Ising components of the spins and the grey arrows, the (smaller) local XY components. The canting does not alter the moment on each tetrahedron relative to the moment with uncanted spins.

cal XY ground states (with continuous degeneracy when three-body interactions are omitted). The range of $\mathcal{J}_{\mathrm{ex}}$ over which the wedge extends increases as Δ decreases. For $\Delta \lesssim 20$ K, the AIAO phase is suppressed entirely because VCFEs increase transverse couplings relative to the Ising couplings (see Fig. 9). We return to this phase diagram in Section V D where we make a comparison of Fig. 13 with the ground states on a cubic unit cell with periodic boundary conditions.

D. Ground states with long-range interactions included - 13 CF states

In the foregoing, we have presented the ground states for H_{eff} derived on a single tetrahedron. For the case of effective nearest neighbor bilinear spin-spin interactions, the single tetrahedron ground states are the same as the four sublattice ($\mathbf{q} = 0$) ground states on the pyrochlore lattice. However, we know that, in the DSIM, obtained from the H_{eff} on a lattice when the crystal field gap Δ is taken to infinity, one of the ground states is a sixteen sublattice configuration (with ordering wavevector $(0, 0, 2\pi/a)$) on a conventional cubic unit cell − the LRSI_{001} state shown in Fig. 1. The long-ranged nature of the dipole-dipole interaction is responsible for the lower energy of the LRSI_{001} state compared to other ordered states that satisfy the local spin ice rules.[41] This observation for the DSIM tells us that we should truncate neither the bare dipole interaction to nearest neighbor nor the effective interactions and that we should not assume $\mathbf{q} = 0$ ordering as was done implicitly in Section V B. Inspired by the case of the DSIM, we investigate the ground states on a cubic unit cell with periodic boundary conditions. The ground states that we find in this section are for the

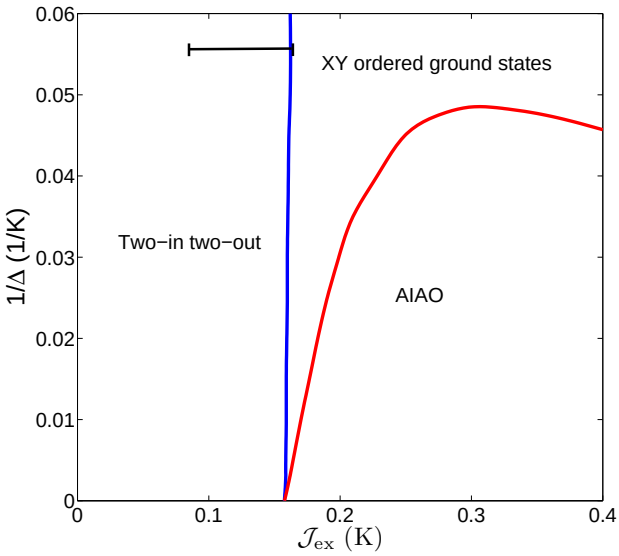

FIG. 13: (color online). Semiclassical ground states of H_{eff} on a periodic cubic unit cell with both bare and effective interactions truncated beyond nearest neighbor. The phase diagram shows the ground states that are obtained over a range of Δ and $\mathcal{J}_{\mathrm{ex}}$. Three body interactions are also neglected. The horizontal bar in the top left hand corner represents the uncertainty in the bare exchange coupling $\mathcal{J}_{\mathrm{ex}}$ in $Tb_2Ti_2O_7$[30,43] at the value of the crystal field gap Δ appropriate to this material.

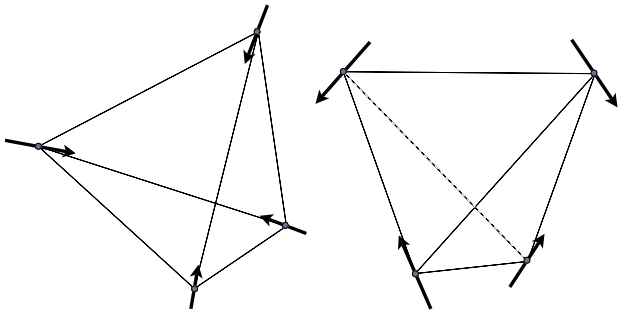

(a) All-in/all-out state. (b) XY configuration.

FIG. 14: A pair of configurations that are ground states of the four sublattice classical analog of the quantum effective Hamiltonian without three-body interactions. The all-in/all-out state (a) occurs for $\mathcal{J}_{\mathrm{ex}} > 0.22$ K and the XY configuration (b) for $0.17 < \mathcal{J}_{\mathrm{ex}} < 0.22$ K.

pyrochlore lattice, assuming that the magnetic unit cell is no bigger than the conventional pyrochlore cubic unit cell (with 16 sites).

For the problem of finding ground states, the effective Hamiltonian is derived in the following way, which differs from the approach presented above in Sections V B and V C in having to treat the long-ranged dipole-dipole interaction. The bare Hamiltonian, which has near-

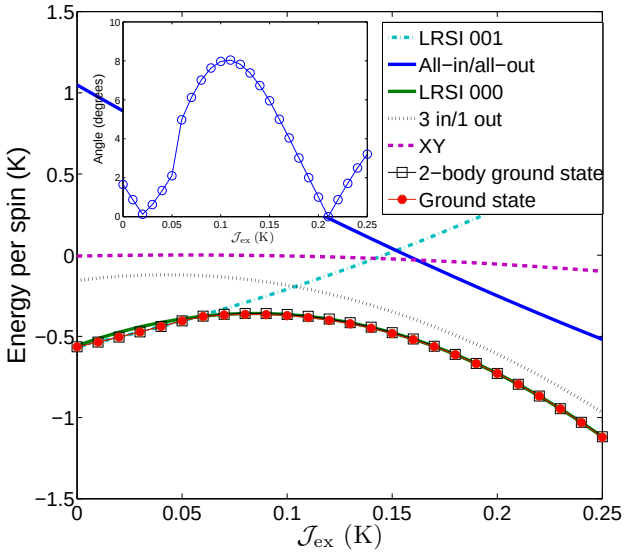

FIG. 15: (color online). Ground state energy for an effective Hamiltonian derived from a model with isotropic exchange and long ranged dipole-dipole interactions on a cubic unit cell with periodic boundary conditions treated by an Ewald summation with $\Delta^{-1} = 0.055$ K^{-1} and $\mathcal{D} = 0.0315$ K. The ground states with (circles) and without (squares) including three-body interactions are shown as well as the energies of different (imposed) spin configurations. The two-body ground states are the LRSI$_{001}$ state for $\mathcal{J}_{ex} \lesssim 0.06$ K which is a two-in/two-out state with ordering wavevector $(0, 0, 2\pi/a)$ and an ordered two-in/two-out state with ordering wavevector $(0, 0, 0)$ for $\mathcal{J}_{ex} \gtrsim 0.06$ K. When three-body terms are included the spins cant out of the Ising directions as indicated in the inset.

est neighbor isotropic exchange and long-ranged dipole-dipole interactions, is computed on a sixteen site cubic unit cell by summing the dipole-dipole interaction over all periodic images by an Ewald summation.[54,76] The effective Hamiltonian is then computed numerically for this periodic model on a cubic unit cell (using identities at the end of Appendix B and summing over the full 13 state crystal field spectrum in the perturbation theory). This procedure preserves the periodicity of the Hamiltonian. One could have instead derived the effective Hamiltonian on a lattice and then sum the interactions over a large but finite lattice assuming periodicity in the classical spin configurations on a cubic unit cell. We present results, in this section, for the former case, but the latter approach gives results that are quantitatively very similar.[77]

The semiclassical ground states energies of the resulting model are computed by replacing the pseudospin operators $(1/2)\sigma^\alpha$ with classical spin components S^α. They are given in Fig. 15 as the bare exchange coupling is varied with $1/\Delta = 0.055$ K^{-1} and $\mathcal{D} = 0.0315$ K; the values appropriate to $Tb_2Ti_2O_7$. In the same figure, we also plot, for comparison, the energies of various imposed (fixed) spin configurations. As in the single tetrahedron case, it is useful to distinguish the ground states obtained when three-body spin interactions are removed and the ground states for the model with all interactions included.

Without three-body spin interactions (open squares in the main panel of Fig. 15) we find that for weakly antiferromagnetic $\mathcal{J}_{ex} \lesssim 0.06$ K, the ground state is the LRSI$_{001}$ state. But, for more antiferromagnetic $\mathcal{J}_{ex}$, instead of the all-in/all-out state found for the DSIM (see inset of Fig. 2), the ground state, at least up to $\mathcal{J}_{ex} = 0.4$ K, is a state with identically ordered tetrahedra (ordering wavevector $\mathbf{q} = 0$) each obeying the ice rules with spins in the local Ising directions − we refer to this as the LRSI$_{000}$ phase.

If the dipole-dipole interaction is cut off at nearest neighbor in the microscopic bare model of Section II A before computing the effective Hamiltonian and if effective couplings beyond nearest neighbors are removed, the LRSI$_{001}$ Ising state has the same energy as the LRSI$_{000}$ Ising phase for $\mathcal{J}_{ex} \lesssim 0.06$ K. The XY phase that we found on a single tetrahedron does not appear in the conventional cubic unit cell model unless all effective interactions are cut off beyond nearest neighbors.

When three-body interactions are restored (filled circles in Fig. 15), the spins cant away from the Ising directions and the energies are lowered relative to the ground states with only two-body interactions considered, similarly to what was found in Section V B on a tetrahedron. The ordering of the Ising components of the spins is the same regardless of whether three-body interactions are present or not. The canting angle of the spins away from the Ising directions is shown as the inset in Fig. 15. There is a maximum in the angle at about $\mathcal{J}_{ex} = 0.11$ K and two minima at about 0.02 K and 0.21 K over the explored range of $\mathcal{J}_{ex}$. The greatest angle is about 8 degrees, compared to 90 degrees in the case of a single tetrahedron. Broadly, the variation in the canting angle follows the magnitude of the three-body coupling (shown for a choice of three sublattices in Fig. 9). The minimum in the canting angle at about $\mathcal{J}_{ex} \sim 0.02$ K coincides with a minimum in the mean squared three-body coupling over all such couplings on the cubic unit cell at this value of the bare exchange. The minimum implies that there is little energy gain to a canting of the spins. The non-monotonic change in the three-body couplings is allowed because the coupling has contributions both quadratic and linear in $\mathcal{J}_{ex}$ coinciding with the exchange-exchange and exchange-dipole contributions to $H_{\rm eff}$ of Eq. (20). The second minimum in the canting angle, $\mathcal{J}_{ex} \approx 0.21$ K, coincides roughly with a vanishing in the three-body coupling (shown in the inset to Fig. 9) and with a change in the sign of the nearest neighbor Ising coupling. We expect therefore, two effects to be at work - a weakening of the three-body coupling and the same effect that suppressed the canting angle in the transition from the XY phase to the AIAO phase on a single tetrahedron (Section V B). The difference in this case is that it is a weak effect compared to that of the

effective further neighbor interactions which control the Ising ordering in this range of couplings. The ordering of the local XY components of the spins is identical to that described in Section V B - one such type of XY ordering is shown in Fig. 12 in which smaller arrows indicate the canting direction away from the Ising directions.[80]

We note in passing that the material $Tb_2Sn_2O_7$ which is, microscopically, very similar to $Tb_2Ti_2O_7$[43] undergoes a phase transition at about 0.87 K to a magnetically long-range ordered phase with ordering wavevector $\mathbf{q} = 0$ and two-in/two-out spin ice configurations on each tetrahedron.[81] The spins in this ordered phase are canted away from the local Ising directions. In these respects, the spin canted LRSI_{000} ground state of the effective Hamiltonian discussed above is similar to the magnetic order in $Tb_2Sn_2O_7$. But the nature of the spin canting differs between the model and the material. The spin canting in $Tb_2Sn_2O_7$ is such as to reduce the moment, on each tetrahedron, compared to the moment if the spins were not canted,[81] whereas the canting of the effective spin 1/2 in the LRSI_{000} state (indicated in Fig. 12) produced by the three-body terms gives a moment, on each tetrahedron, that is the same as the moment of the LRSI_{000} configuration without spin canting.

The classical DSIM (which is recovered for an infinite ground to first excited crystal field gap, Δ) with long range dipole-dipole interactions has a phase boundary between the LRSI_{001} spin ice configurations and all-in/all-out states at about $\mathcal{J}_{\text{ex}} = 0.14$ K (see inset of Fig. 2). We have seen that, in the effective model of $Tb_2Ti_2O_7$, the semiclassical ground states, at least for $\mathcal{J}_{\text{ex}} < 0.25$ K, are spin ice configurations although the bare exchange coupling $\mathcal{J}_{\text{ex}}$ is antiferromagnetic so we see that spin ice correlations are favored by VCFEs. However, Fig. 9 shows that the average nearest neighbor Ising exchange J^{zz} swaps sign at about 0.2 K so the persistence of ice-like correlations in $Tb_2Ti_2O_7$, in the form of the LRSI_{000} state, up to, at least, $\mathcal{J}_{\text{ex}} = 0.4$ K (see Fig. 2) is not due to the renormalization of the Ising exchange described in Section IV G but is induced by further neighbor couplings. The effective Hamiltonian to order $\Delta(\mathcal{J}_{\text{ex}}/\Delta)^2$ is therefore a novel two-in/two-out model that does not rely on nearest neighbor interactions to produce ice-like correlations.

To shed some light on the fact that the all-in/all-out state, (Fig. 14(a)), observed on a single tetrahedron and in the DSIM,[41,45,48] is not seen in the sixteen sublattice case, (for the value $1/\Delta \approx 0.055$ K^{-1} as shown in Fig. 2 and Fig. 15), we have computed the semiclassical ground states for a range of Δ and bare exchange couplings for the sixteen sublattice effective Hamiltonian on a cubic unit cell with periodic boundary conditions. We have omitted the three spin interactions which are not responsible for the presence of the LRSI_{000} state. The result is shown in Fig. 2. This is the main result of our paper.

For $\Delta \gtrsim 340$ K ($1/\Delta \lesssim 0.003$), the phases are those of the DSIM with a phase boundary at about $\mathcal{J}_{\text{ex}} = 0.14$ K when $1/\Delta = 0$. For comparison, we include an inset showing the classical DSIM phase diagram for $\mathcal{D} = 0.0315$ K.[41,48] As the gap Δ is lowered from infinity, a $\mathbf{q} = 0$ LRSI_{000} phase − appears at about $\Delta \sim 340$ K.[82] As Δ is lowered further, the range of $\mathcal{J}_{\text{ex}}$ over which this LRSI_{000} phase is observed increases − the spin-spin interactions arising from VCFEs stabilizing the LRSI_{000} state. Indeed, for $\Delta \lesssim 29$ K ($1/\Delta \sim 0.035$ K^{-1}), there is no all-in/all-out phase at least for any $\mathcal{J}_{\text{ex}} < 0.4$ K.

Over the range of $\mathcal{J}_{\text{ex}}$ explored here, the LRSI_{000} phase boundary has a dip with a minimum at about $\mathcal{J}_{\text{ex}} = 0.14$ K. The LRSI_{000} is not observed in the DSIM so the quantum terms of $H_{\text{eff}}^{(2)}$ is responsible for its existence. Therefore $\mathcal{J}_{\text{ex}} = 0.14$ K is the exchange coupling at which the effect of the classical term is minimized because the isotropic exchange and the dipole-dipole contributions to the Ising exchange almost cancel each other. This accounts for the "tail" in Fig 2 where the LRSI_{001} to LRSI_{000} phase boundary extends to $1/\Delta \sim 0.005$ K^{-1} − the quantum terms are dominant at about $\mathcal{J}_{\text{ex}} = 0.14$ K. The phase diagram in Fig. 2 shows that for $\mathcal{J}_{\text{ex}} \gtrsim 0.25$ K, the LRSI_{000} spin ice appears over a larger range of $1/\Delta$. This is because for larger values of the exchange, the quantum terms are larger for a given Δ and also because the quantum terms vary as $\mathcal{J}_{\text{ex}}^2$ they eventually dominate over the classical terms.

These observations lead us to two comments. Firstly, the shape of the LRSI_{000} phase boundary in Fig. 2 is similar to the shape of the phase boundary for nearest neighbor bare and effective interactions shown in Fig. 13. The explanation we have given earlier in this Section V D (for the case with long-range dipoles on a cubic unit cell) for the shape of this boundary is equally applicable to the case with nearest neighbor bare and effective interactions discussed in Section V C. A comparison of these two figures reveals that, whereas quantum terms strongly influence the nearest neighbor phase diagram enough to produce an XY phase, the replacement of this phase by LRSI_{000} requires interactions beyond nearest neighbor which, therefore, should not be neglected.

Secondly, as $\mathcal{J}_{\text{ex}}/\Delta$ increases, eventually higher order terms in powers of $\mathcal{J}_{\text{ex}}/\Delta$ must become important and our effective model will break down. It is possible that the inclusion of higher order terms would lead to the all-in/all-out phase persisting to larger values of $1/\Delta$ than we find considering only the lowest order quantum corrections $H_{\text{eff}}^{(2)}$ to the DSIM. Fig. 3 is a comparison of the exact four state model of Eq. (27) with the effective Hamiltonian on a single tetrahedron. The singlet-doublet phase boundary indicates that the AIAO phase region should occupy a larger range of $1/\Delta$ as $\mathcal{J}_{\text{ex}}$ increases than is borne out by the semiclassical ground state calculation on a single tetrahedron (Fig. 11). On the basis of this comparison alone, however, one cannot draw any conclusions about the effect of higher order corrections on the phase diagram of the effective Hamiltonian on a lattice.

VI. SUMMARY AND DISCUSSION

In this paper, we have introduced a low energy effective Hamiltonian for $Tb_2Ti_2O_7$ formally derived from a minimal microscopic bare Hamiltonian. The bare model consists of a crystal field Hamiltonian for each magnetic ion and isotropic exchange and dipole-dipole interactions between the J = 6 angular momenta (Eq. (1) and discussion in Section II A). The low energy model is expressed in terms of effective spin one-half operators which operate on states in the two dimensional Hilbert space spanned by the single ion ground state crystal field doublet on each magnetic site. The effective theory is obtained as a perturbation expansion in $\langle V\rangle/\Delta$ where $\langle V\rangle$ is the characteristic energy scale of the spin-spin interactions which incorporate exchange and dipole-dipole coupling,[44] and Δ is the energy gap between the ground and first excited levels in the crystal field spectrum. In Section II, we gave a detailed discussion of the terms that arise in the effective model to lowest order in the quantum corrections. To first order in the effective Hamiltonian in powers of $\langle V\rangle/\Delta$ is the DSIM[41,45,68] which has only interactions between the Ising components of the pseudospins. This model on its own has an antiferromagnetic all-in/all-out (AIAO) ground state for the estimated bare exchange, dipolar and crystal field parameters for $Tb_2Ti_2O_7$ (see vertical dashed line in the inset to Fig. 2). The next (second) order in $\langle V\rangle/\Delta$ includes the lowest order quantum fluctuations involving virtual transitions into excited crystal field levels. We found that the introduction of these virtual fluctuations leads to a renormalization of the effective Ising exchange coupling in $H_{\rm eff}$ of the lowest order (spin ice) model in such a way that two-in/two-out Ising configurations are favored on the single tetrahedron over a wider range of $\mathcal{J}_{\rm ex}$ than one would find from the lowest order (DSIM) model. Also, to second order in $\langle V\rangle/\Delta$, various anisotropic transverse effective exchange couplings appear (in addition to corrections to the effective Ising exchange) as well as some three-body interactions. Broadly speaking, the interactions between the effective spins become less Ising-like in the presence of virtual crystal field excitations (VCFEs). This behavior is also borne out by comparisons of the diffuse neutron scattering pattern for $Tb_2Ti_2O_7$[26,27,28,53] with both classical mean field theory with classical Heisenberg spins and finite Ising-like anisotropy[54] and by RPA calculations starting from the bare microscopic model presented in Section II A.[55] In other words, the conclusion reached in Ref. 33 that, on the basis of exact diagonalization calculations and perturbation theory calculations on a single tetrahedron, $Tb_2Ti_2O_7$ may perhaps be described by a soft (quantum) spin ice system is upheld by the work presented in the present paper.

We studied the properties of the low energy (effective) Hamiltonian $H_{\rm eff}$ by finding the ground states, as a function of bare isotropic exchange couplings $\mathcal{J}_{\rm ex}$ (from the model in Eq. (5)), and for the crystal field spectrum of $Tb_2Ti_2O_7$, under the assumption that the pseudospins are classical (i.e. the pseudospins are vectors of fixed length $S = 1/2$). Truncating the bare Hamiltonian and then the effective Hamiltonian to nearest neighbor interactions and assuming ground states with ordering wavevector of $\mathbf{q} = 0$ (identical spin configurations on elementary tetrahedra on the pyrochlore lattice) and omitting three spin interactions, we found three different semiclassical ground states depending on the ratio $\mathcal{J}_{\rm ex}/\mathcal{D}$ (see Eq. (18)). Specifically, we found (i) a two-in/two-out state and (ii) an all-in/all-out state. In addition to these two states is one with spins lying in the local XY planes perpendicular to the [111] directions (see, for example, Fig. 14(b)) with a continuous degeneracy.

If, instead, the original model has long-ranged dipolar interactions treated by an Ewald summation on a single cubic unit cell, then the effective Hamiltonian has interactions with the periodicity of a cubic unit cell. For such a model, again without three spin interactions, (and assuming that the magnetic unit cell is not larger than a single cubic unit cell), we find (for $1/\Delta = 0.055$ K^{-1} relevant to $Tb_2Ti_2O_7$) two semiclassical ground states. For weakly antiferromagnetic bare exchange, $\mathcal{J}_{\rm ex}$, the ground state is the $\rm LRSI_{001}$ phase (see Fig. 1) − a ground state of the dipolar ice model − and, for more antiferromagnetic $\mathcal{J}_{\rm ex}$, the ground state is a two-in/two-out state with propagation (ordering) wavevector $\mathbf{q} = 0$. The latter result − the persistence of spin ice correlations with antiferromagnetic bare coupling − is partly a consequence of the renormalization of the effective Ising exchange coupling which includes contributions from the bare dipole coupling $\mathcal{D}$ and the bare isotropic exchange coupling $\mathcal{J}_{\rm ex}$. It is also partly due to the presence of further neighbor interactions not present in the microscopic model. Because spin ice-like correlations appear over a wider range of couplings than one would find in the classical model, the VCFEs are responsible for frustrating the interactions in our simplified model (see Eqs. (1),(2) and (5)) of $Tb_2Ti_2O_7$.

When the three-body interactions are incorporated, the ordering of the Ising components of the spins is not changed from the results without three-body terms, but the effective spins then become canted out of the local Ising directions and the local XY components are ordered into the so-called ψ_2 states (see Fig. 12).[14,63,79] This XY ordering is observed in the easy plane antiferromagnetic $Er_2Ti_2O_7$. However, we note that the effective Hamiltonian for $Er_2Ti_2O_7$ has no three-body interactions (a consequence of time reversal within a Kramers doublet) so the effective Hamiltonian for $Er_2Ti_2O_7$ cannot account for the observed ordered state by means of three-body interactions.

Returning to $Tb_2Ti_2O_7$, in the present work we have established that VCFEs can be included as a significant perturbation to the DSIM and that the interactions induced by VCFEs have an important effect on the physics of this material. By far the most important problems now remaining are to establish the ground state and low energy excitations of the fully quantum effective Hamil-

tonian derived in this paper beyond the single tetrahedron approximation (see Section IV G) and to assess the importance of higher order terms in the perturbation expansion. This might be accomplished by pursuing exact diagonalization or series expansions.[56]

Further unresolved problems are to account for the long-range order in $Tb_2Ti_2O_7$ that is induced by a [110] magnetic field[83] and by applying pressure.[84] There is also evidence to suggest that there are dynamical lattice distortions away from a pyrochlore structure in zero magnetic field.[85,86] However, the extent to which these affect or are affected by the magnetism in the material is not known. With the availability of an effective Hamiltonian that considers the effect of excited crystal field levels in $Tb_2Ti_2O_7$, one can perhaps hope to supplement the model to explore the role of the lattice on the magnetism of $Tb_2Ti_2O_7$ and $Tb_2Sn_2O_7$.

One could extend the work in this article by including interactions in the bare Hamiltonian besides isotropic exchange and dipole-dipole interactions. For example, one could explore the effect of generalized anisotropic nearest neighbor exchange interactions as was done at the mean field level in Ref. 87 (for $Yb_2Ti_2O_7$) and Ref. 63 (for $Er_2Ti_2O_7$). In addition, one could include further neighbor interactions in the bare Hamiltonian. It is already known that further neighbor interactions are present in the related (spin ice) material $Dy_2Ti_2O_7$.[47] If further neighbor interactions were shown to be significant in $Tb_2Ti_2O_7$, they could be incorporated following the approach in this article.

Looking beyond the question of the ground state of $Tb_2Ti_2O_7$, we point out that an effective Hamiltonian of the type described in this article might find a use in other problems on magnetic systems. For example, this approach might find some use in studying the material $Pr_2Sn_2O_7$ [88] which has been referred to as "dynamic spin ice" with an ill-understood fast dynamics compared to $Ho_2Ti_2O_7$. Two other pyrochlore magnets with Ising-like crystal field ground states are the metallic spin ice $Pr_2Ir_2O_7$ [89] and the material $Pr_2Zr_2O_7$ [90] both of which exhibit no long range magnetic order at low temperature. Finally, we mention another material for which the effective Hamiltonian formalism might be useful − the langasites $Nd_3Ga_5SiO_{14}$[24,91,92,93] and $Pr_3Ga_5SiO_{14}$.[92,94] These materials show no sign of order at least down to 35 mK although the scale of the interactions in both compounds is much larger, as read off from the Curie-Weiss temperatures (−52 K and −2.3 K for $Nd_3Ga_5SiO_{14}$[91,92] and $Pr_3Ga_5SiO_{14}$[95] respectively).

We hope that the present work stimulates further theoretical investigation into the exotic and interesting behavior displayed by these materials.

Acknowledgments

We thank Benjamin Canals, Matt Enjalran, Tom Fennell, Ludovic Jaubert and Jacob Ruff for their critical reading of the manuscript. This research was funded by the NSERC of Canada and the Canada Research Chair program (M. G., Tier I), the Emerging Materials Knowledge of Materials Manufacturing Ontario, the Canada Foundation for Innovation and the Ontario Innovation Trust.

APPENDIX A: EFFECTIVE HAMILTONIAN

In order to keep this paper self-contained, and in the hope that the approach we have followed here will be of use to others, we sketch out the main ideas behind the derivation of the effective Hamiltonian. The discussion, which we keep fairly general, roughly follows Ref. 65 to which we refer for a broader context.

We consider a quantum mechanical system described by Hamiltonian H which can be split into H_0 plus a small perturbation V. We label the exact eigenstates of H by $|\Psi_n\rangle$ which corresponds to eigenvalue E_n for n from 1 to the dimension of the Hilbert space $\mathcal{N}$. The eigenstates of the Hamiltonian H_0 are denoted $|n_0\rangle$ (where the integer n labels different eigenstates) and satisfy

$$H_0|n_0\rangle = E_{0,n}|n_0\rangle.$$

In the following, we imagine that the ground state of H_0 is p-fold degenerate and that eigenstates are labeled $|1_0\rangle$ to $|p_0\rangle$ and have energy E_0. When we introduce the perturbation V, to zeroth order in ordinary degenerate perturbation theory, the ground state wavefunctions are some particular admixtures of these degenerate states − in this sense they are strongly coupled by the perturbation.

We wish to set up a Hamiltonian that "lives" in the subspace spanned by the ground state levels of H_0 and which includes the effect of V on these levels. Therefore, we introduce a projector $\mathcal{P}$ that projects onto this subspace. Given an exact state $|\Psi_n\rangle$,

$$\mathcal{P}|\Psi_n\rangle \equiv |\Psi_{0,n}\rangle$$

where $|\Psi_{0,n}\rangle$ is a linear combination of $|n_0\rangle$ for $n = 1, \ldots, p$. We refer to this subspace as the model space $\mathfrak{M}$. Because the perturbation is assumed to be weak, the exact eigenstates $|\Psi_n\rangle$, for n from 1 to p lie mainly within $\mathfrak{M}$. We also introduce an operator Ω that "undoes" the effect of the projector $\mathcal{P}$,

$$\Omega|\Psi_{0,n}\rangle \equiv |\Psi_n\rangle.$$

It follows that $|\Psi_{0,n}\rangle = \mathcal{P}\Omega|\Psi_{0,n}\rangle$ and, because this equation is satisfied by any linear combination of the exact states $|\Psi_{0,n}\rangle$, we find that $\mathcal{P}\Omega\mathcal{P} = \mathcal{P}$.

The following intermediate result holds:

$$[\Omega, H_0]\mathcal{P} = V\Omega\mathcal{P} - \Omega\mathcal{P}V\Omega\mathcal{P}. \tag{A1}$$

To see this, begin with the Schrödinger equation in the form $(E_n - H_0)|\Psi_n\rangle = V|\Psi_n\rangle$ and multiply (from the

left) by $\mathcal{P}$ to get

$$(E_n - H_0)|\Psi_{0,n}\rangle = \mathcal{P}V|\Psi_n\rangle$$

because the projector commutes with the Hamiltonian H_0.

The effective Hamiltonian, $H_{\rm eff}$, is defined to be

$$H_{\rm eff} \equiv \mathcal{P}H\Omega\mathcal{P} \tag{A2}$$

which has the property

$$H_{\rm eff}|\Psi_{0,n}\rangle = E_n|\Psi_{0,n}\rangle.$$

The effective Hamiltonian has eigenstates living in the model space $\mathfrak{M}$ and has as eigenvalues the exact eigenvalues. The projector on the right-hand-side is there to ensure that the remaining operators $\mathcal{P}H\Omega$ operate on the model space, $\mathfrak{M}$. Operationally, in Eq. (A2), the Ω operator rotates the model space state into an exact eigenstate. H produces the exact eigenvalue and then the exact eigenstate is projected back into the model space.

We compute $H_{\rm eff}$ in perturbation theory by expanding Ω implicitly in powers of V

$$\Omega = 1 + \Omega^{(1)} + \Omega^{(2)} + \ldots \tag{A3}$$

It is then possible to eliminate $\Omega^{(k)}$ by introducing the so-called resolvent operator

$$\mathcal{R} \equiv (E_0 - H_0)^{-1}\mathcal{Q}$$

where $\mathcal{Q} = \mathbb{I} - \mathcal{P}$. The resolvent has the spectral representation

$$\mathcal{R} = \sum_{|\psi\rangle\notin\mathcal{M}} \frac{|\psi\rangle\langle\psi|}{E_0 - E_\psi}.$$

Note that $\mathcal{R} = \mathcal{R}\mathcal{Q}$.

To eliminate $\Omega^{(k)}$, introduce the series (A3) into identity (A1) and use the fact that $\mathcal{P}$ projects onto states with the same H_0 eigenvalue E_0 to obtain

$$\Omega^{(1)}\mathcal{P} = \mathcal{R}V\mathcal{P}$$
$$\Omega^{(2)}\mathcal{P} = \mathcal{R}(V\Omega^{(1)}\mathcal{P} - \Omega^{(1)}\mathcal{P}V\mathcal{P})$$

and so on. These recursion relations can be solved to get $\Omega^{(k)}$ in terms of $\mathcal{R}$, V and $\mathcal{P}$.

The effective Hamiltonian (A2) then takes the form

$$H_{\rm eff} = \mathcal{P}H\mathcal{P} + \mathcal{P}H\mathcal{R}H\mathcal{P} + \ldots$$

which, in turn, is

$$H_{\rm eff} = \mathcal{P}H_0\mathcal{P} + \mathcal{P}V\mathcal{P} + \mathcal{P}V\mathcal{R}V\mathcal{P} + \ldots$$

because, in term $\mathcal{P}H\mathcal{R}H\mathcal{P}$, the unperturbed Hamiltonian is eliminated because it does not contain any terms that connect the model space with the space orthogonal to it − that is, terms like $\mathcal{P}H_0\mathcal{R}H\mathcal{P}$ vanish.

APPENDIX B: CALCULATIONS FOR CASE A

In this appendix, we give more details of the calculation leading to the effective pseudospin interactions from $H_{\rm eff}^{(2)}$ which is that part of the effective Hamiltonian that includes VCFEs to lowest order in $\langle V\rangle/\Delta$. We begin with Eq. (21) which we reproduce below

$$\sum_{\alpha,\beta,\rho,\sigma}\sum_{m_p}\sum_{W}\mathcal{P}(m_1,m_2,m_3)\tilde{\mathcal{K}}^{\alpha\beta}_{I_1I_2}\widetilde{J}^{\alpha}_{I_1}\widetilde{J}^{\beta}_{I_2} \times \frac{|m_{I_1,4},W_{I_2},m_{I_3,3}\rangle\langle m_{I_1,4},W_{I_2},m_{I_3,3}|}{E_0 - E_W} \times \tilde{\mathcal{K}}^{\rho\sigma}_{I_2I_3}\widetilde{J}^{\rho}_{I_2}\widetilde{J}^{\sigma}_{I_3}\mathcal{P}(m_4,m_5,m_6). \tag{B1}$$

In this formula, the lattice sites I_1, I_2 and I_3 have been fixed. We observe that the matrix elements for the angular momenta on sites I_1 and I_3 are taken between states within the ground state crystal field doublet. The nonvanishing matrix elements within this doublet are given in Eq. (4). From this equation, we see that α and σ must equal z. We consider the operators in Eq. (B1) that act on site I_1

$$\sum_{m_1,m_4}|m_1\rangle\langle m_1|\widetilde{J}^z_{I_1}|m_4\rangle\langle m_4| \longrightarrow |1\rangle\langle 1|\langle 1|\widetilde{J}^z_{I_1}|1\rangle + |2\rangle\langle 2|\langle 2|\widetilde{J}^z_{I_1}|2\rangle = -\langle\widetilde{J}^z_{I_1}\rangle\left(|1\rangle\langle 1| - |2\rangle\langle 2|\right) \to -\langle\widetilde{J}^z_{I_1}\rangle\tilde{\sigma}^z_{I_1}.$$

A similar calculation gives $-\langle\tilde{J}^z\rangle\tilde{\sigma}^z$ on site I_3. Eq. (B1) becomes

$$\sum_{\beta,\rho}\tilde{\mathcal{K}}^{z\beta}_{I_1I_2}\tilde{\mathcal{K}}^{\rho z}_{I_2I_3}\langle\widetilde{J}^z\rangle^2\tilde{\sigma}^z_{I_1}\tilde{\sigma}^z_{I_3} \times\left(\sum_{m_2,m_5}\sum_{W}|m_2\rangle\langle m_5|\frac{\langle m_2|\widetilde{J}^{\beta}_{I_2}|W\rangle\langle W|\widetilde{J}^{\rho}_{I_2}|m_5\rangle}{E_0 - E_W}\right). \tag{B2}$$

The sum over W runs over all single ion crystal field excited states. We will consider only the sum over the lowest excited crystal field doublet states: $|3\rangle$ and $|4\rangle$. The denominator $E_W - E_0$ equals Δ. The relevant matrix elements are, from exact diagonalization of the crystal field Hamiltonian,

$$\langle 1|\widetilde{J}^x|3\rangle \equiv A$$
$$\langle 1|\widetilde{J}^y|3\rangle \equiv -iA$$
$$\langle 1|\widetilde{J}^z|4\rangle \equiv B$$
$$\langle 2|\widetilde{J}^z|3\rangle \equiv -B$$
$$\langle 2|\widetilde{J}^x|4\rangle \equiv -A$$
$$\langle 2|\widetilde{J}^y|4\rangle \equiv -iA.$$

All other matrix elements vanish. We shall not make any assumptions about the form of $\tilde{\mathcal{K}}^{\alpha\beta}_{I_2,I_3}$ except for symmetry under swapping both pairs of indices. The sums in

brackets in Eq. (B2) give the operators

$$\begin{aligned}
&|1\rangle\langle 2|\left(-\tilde{\mathcal{K}}^{zx}_{I_1I_2}\tilde{\mathcal{K}}^{zz}_{I_2I_3}+i\tilde{\mathcal{K}}^{zy}_{I_1I_2}\tilde{\mathcal{K}}^{zz}_{I_2I_3}-\tilde{\mathcal{K}}^{zz}_{I_1I_2}\tilde{\mathcal{K}}^{xz}_{I_2I_3}\right.\\
&\qquad\left.+i\tilde{\mathcal{K}}^{zz}_{I_1I_2}\tilde{\mathcal{K}}^{yz}_{I_2I_3}\right)AB\\
&+|2\rangle\langle 1|\left(-\tilde{\mathcal{K}}^{zz}_{I_1I_2}\tilde{\mathcal{K}}^{xz}_{I_2I_3}-i\tilde{\mathcal{K}}^{zz}_{I_1I_2}\tilde{\mathcal{K}}^{yz}_{I_2I_3}-\tilde{\mathcal{K}}^{zx}_{I_1I_2}\tilde{\mathcal{K}}^{zz}_{I_2I_3}\right.\\
&\qquad\left.-i\tilde{\mathcal{K}}^{zy}_{I_1I_2}\tilde{\mathcal{K}}^{zz}_{I_2I_3}\right)AB\\
&+|1\rangle\langle 1|\left(\left(\tilde{\mathcal{K}}^{zx}_{I_1I_2}\tilde{\mathcal{K}}^{xz}_{I_2I_3}+\tilde{\mathcal{K}}^{zy}_{I_1I_2}\tilde{\mathcal{K}}^{yz}_{I_2I_3}+i\tilde{\mathcal{K}}^{zx}_{I_1I_2}\tilde{\mathcal{K}}^{yz}_{I_2I_3}\right.\right.\\
&\qquad\left.\left.-i\tilde{\mathcal{K}}^{zy}_{I_1I_2}\tilde{\mathcal{K}}^{xz}_{I_2I_3}\right)A^2+\tilde{\mathcal{K}}^{zz}_{I_1I_2}\tilde{\mathcal{K}}^{zz}_{I_2I_3}B^2\right)\\
&+|2\rangle\langle 2|\left(\left(\tilde{\mathcal{K}}^{zx}_{I_1I_2}\tilde{\mathcal{K}}^{xz}_{I_2I_3}+\tilde{\mathcal{K}}^{zy}_{I_1I_2}\tilde{\mathcal{K}}^{yz}_{I_2I_3}-i\tilde{\mathcal{K}}^{zx}_{I_1I_2}\tilde{\mathcal{K}}^{yz}_{I_2I_3}\right.\right.\\
&\qquad\left.\left.+i\tilde{\mathcal{K}}^{zy}_{I_1I_2}\tilde{\mathcal{K}}^{xz}_{I_2I_3}\right)A^2+\tilde{\mathcal{K}}^{zz}_{I_1I_2}\tilde{\mathcal{K}}^{zz}_{I_2I_3}B^2\right). \quad \text{(B3)}
\end{aligned}$$

Of these four operators, the top two involve virtual excitations on ion I_2 that do not return the ion to its original state but instead take it into the other crystal field ground state on ion I_2 − an overall Ising spin flip. We shall see that, as we should expect, these spin flip operations correspond to $\tilde{\sigma}^x$ or $\tilde{\sigma}^y$ effective operators. This leads us to an important point - in order for $\tilde{\sigma}^x$ or $\tilde{\sigma}^y$ effective operators to be significant in the effective Hamiltonian for $Tb_2Ti_2O_7$, there must be nonvanishing $\tilde{J}^x$, $\tilde{J}^y$ *and* $\tilde{J}^z$ matrix elements between the ground state doublet and first excited doublet. In order for this to be the case, the ground state and first excited wavefunctions, which have the form

$$|n\rangle=\sum_{M=-J}^{J}|J,M\rangle$$

cannot have only the predominant $|J,\pm 4\rangle$ (in the ground doublet) and $|J,\pm 5\rangle$ (in the first excited doublet) coefficients for then the $\tilde{J}^z$ matrix elements would vanish. Hence the conclusions of the paper are unlikely to carry over to other materials, for example, to the spin ices.

Referring to Eq. (11), we find that the above operators in Eq. (B3) can be re-expressed in terms of Pauli matrices. So the result of the sum of excited crystal field states in Eq. (B2) is

$$\begin{aligned}
&\left(\tilde{\mathcal{K}}^{zz}_{I_1I_2}\tilde{\mathcal{K}}^{zz}_{I_2I_3}B^2+\tilde{\mathcal{K}}^{zx}_{I_1I_2}\tilde{\mathcal{K}}^{xz}_{I_2I_3}A^2+\tilde{\mathcal{K}}^{zy}_{I_1I_2}\tilde{\mathcal{K}}^{yz}_{I_2I_3}A^2\right)\mathbb{I}_{I_2}\\
&\quad+\left(\tilde{\mathcal{K}}^{zx}_{I_1I_2}\tilde{\mathcal{K}}^{yz}_{I_2I_3}A^2-\tilde{\mathcal{K}}^{zy}_{I_1I_2}\tilde{\mathcal{K}}^{xz}_{I_2I_3}A^2\right)i\tilde{\sigma}^z_{I_2}\\
&\quad-\left(\tilde{\mathcal{K}}^{zz}_{I_1I_2}\tilde{\mathcal{K}}^{xz}_{I_2I_3}+\tilde{\mathcal{K}}^{zx}_{I_1I_2}\tilde{\mathcal{K}}^{zz}_{I_2I_3}\right)AB\tilde{\sigma}^x_{I_2}\\
&\quad-\left(\tilde{\mathcal{K}}^{zy}_{I_1I_2}\tilde{\mathcal{K}}^{zz}_{I_2I_3}+\tilde{\mathcal{K}}^{zz}_{I_1I_2}\tilde{\mathcal{K}}^{yz}_{I_2I_3}\right)AB\tilde{\sigma}^y_{I_2}. \quad \text{(B4)}
\end{aligned}$$

After substituting the couplings $\tilde{\mathcal{K}}$ we find that the $\tilde{\sigma}^z$ terms vanish. The resulting expression is time-reversal invariant. Incorporating Eq. (B4) into Eq. (B2), we find that the overall interactions are, as we stated in the main text, Ising interactions $\tilde{\sigma}^z_{I_1}\tilde{\sigma}^z_{I_3}$ (arising from the unit operator in Eq. (B4)) and three-body interactions of the form $\tilde{\sigma}^z_{I_1}\tilde{\sigma}^\alpha_{I_2}\tilde{\sigma}^z_{I_3}$ with $\alpha=x,y$. Having determined the general form of the interactions and their couplings, we carry out a sum over all lattice sites I_1, I_2 and I_3. The calculations for Cases B and C in the main text are carried out in a similar manner.

In order to organize the calculation of the terms in the effective Hamiltonian, all sums over virtual excited states and lattice sites are carried out numerically and the calculations described in this appendix are performed by exploiting the orthogonality of the Pauli matrices. As an example, suppose that the operator coefficients in Eq. (B1) have been evaluated in the $|1\rangle$, $|2\rangle$ basis. We call this operator $\hat{O}$. We want to decompose this operator into a sum of the form

$$\sum_{a,b,c}A_{abc}\tilde{\sigma}^a\tilde{\sigma}^b\tilde{\sigma}^c$$

where the sum runs over the Pauli operators $\tilde{\sigma}^x$, $\tilde{\sigma}^y$, $\tilde{\sigma}^z$,and the unit operator. Coefficients A_{abc} are determined from

$$A_{abc}=\frac{1}{8}\mathrm{Tr}[\hat{O}\tilde{\sigma}^a\tilde{\sigma}^b\tilde{\sigma}^c].$$

This formula is sufficient for Case A (Section IV B) with operators on three pyrochlore sites I_1, I_2 and I_3. For Cases B and C (Sections IV C and IV D), we decompose into a sum

$$\sum_{a,b}B_{ab}\tilde{\sigma}^a\tilde{\sigma}^b$$

using

$$B_{ab}=\frac{1}{4}\mathrm{Tr}[\hat{O}\,\tilde{\sigma}^a\tilde{\sigma}^b].$$

APPENDIX C: CRYSTAL FIELD PARAMETERS FOR $Tb_2Ti_2O_7$

The crystal field parameters for $Tb_2Ti_2O_7$ are obtained from those found for $Ho_2Ti_2O_7$ in Ref. 42 from the formula 3. Ref. 42 uses the convention

$$H_{\mathrm{cf}}=\sum_l\sum_{m=-l}^{l}\bar{B}^m_l\left(\frac{4\pi}{2l+1}\right)^{1/2}Y^m_l$$

for the crystal field parameters. One can convert the set of $\bar{B}^m_l$ to the B^m_l using the parameters given in Ref. 96 and the matrix elements of Table II.

The $Ho_2Ti_2O_7$ crystal field parameters are:

$$\begin{aligned}
&\tfrac{B^0_2}{(S_2)_{\mathrm{Ho}}}=791\mathrm{K}\quad \tfrac{B^0_4}{(S_4)_{\mathrm{Ho}}}=3189\mathrm{K}\quad \tfrac{B^0_6}{(S_6)_{\mathrm{Ho}}}=1007\mathrm{K}\\
&\tfrac{B^3_4}{(S_4)_{\mathrm{Ho}}}=739\mathrm{K}\quad \tfrac{B^3_6}{(S_6)_{\mathrm{Ho}}}=-725\mathrm{K}\quad \tfrac{B^6_6}{(S_6)_{\mathrm{Ho}}}=1179\mathrm{K}. \quad \text{(C1)}
\end{aligned}$$

The radial expectation values $\langle r^m\rangle$ are given in Table II [59] and the Stevens factors for $Tb_2Ti_2O_7$ are given in Table III[58]

TABLE II: Table of radial expectation values, $\langle r^m \rangle$, for $Tb_2Ti_2O_7$ and $Ho_2Ti_2O_7$.[59]

R^{3+}	$\langle \mathbf{r}^2 \rangle$	$\langle \mathbf{r}^4 \rangle$	$\langle \mathbf{r}^6 \rangle$
Ho	0.7446	1.3790	5.3790
Tb	0.8220	1.6510	6.8520

TABLE III: Table of Stevens factors for $Tb_2Ti_2O_7$ and $Ho_2Ti_2O_7$.[97]

R^{3+}	$S_2(\times 10^2)$	$S_4(\times 10^4)$	$S_6(\times 10^6)$
Ho	-0.2222	-0.3330	-1.2937
Tb	-1.0101	1.2244	-1.1212

[1] S. T. Bramwell and M. J. P. Gingras, Science **294**, 1495 (2001).
[2] M. J. P. Gingras, arXiv:0903.2772.
[3] S. T. Bramwell, M. J. P. Gingras, and P. C. W. Holdsworth, Frustrated Spin Systems (H. T. Diep, World Scientific, 2004).
[4] J. R. Schrieffer and P. A. Wolff, Phys. Rev. **149**, 491 (1966).
[5] J. Villain, Z. Phys. **B33**, 31 (1979).
[6] R. Moessner and J. T. Chalker, Phys. Rev. Lett. **80**, 2929 (1998).
[7] R. Moessner and J. T. Chalker, Phys. Rev. B **58**, 12049 (1998).
[8] J. N. Reimers, Phys. Rev. B **45**, 7287 (1992).
[9] J. N. Reimers, A. J. Berlinsky, and A. C. Shi, Phys. Rev. B **43**, 865 (1991).
[10] J. S. Gardner, M. J. P. Gingras, and J. E. Greedan, arXiv:0903.3661 (to appear in Rev. Mod. Phys.).
[11] S. E. Palmer and J. T. Chalker, Phys. Rev. B **62**, 488 (2000).
[12] M. Elhajal, B. Canals, R. Sunyer, and C. Lacroix, Phys. Rev. B **71**, 094420 (2005).
[13] J. D. M. Champion, M. J. Harris, P. C. W. Holdsworth, A. S. Wills, G. Balakrishnan, S. T. Bramwell, E. Cizmar, T. Fennell, J. S. Gardner, J. Lago, et al., Phys. Rev. B **68**, 020401 (2003).
[14] J. D. M. Champion and P. C. W. Holdsworth, J. Phys.: Condens. Matter **16**, S665 (2004).
[15] J. D. M. Champion, A. S. Wills, T. Fennell, S. T. Bramwell, J. S. Gardner, and M. A. Green, Phys. Rev. B **64**, 140407(R) (2001).
[16] J. R. Stewart, G. Ehlers, A. S. Wills, S. T. Bramwell, and J. S. Gardner, J. Phys.: Condens. Matter **16**, L321 (2004).
[17] A. S. Wills, M. E. Zhitomirsky, B. Canals, J. P. Sanchez, P. Bonville, P. D. de Reotier, and A. Yaouanc, J. Phys.: Condens. Matter **18**, L37 (2006).
[18] M. J. P. Gingras, C. V. Stager, N. P. Raju, B. D. Gaulin, and J. E. Greedan, Phys. Rev. Lett. **78**, 947 (1997).
[19] J. S. Gardner, B. D. Gaulin, S.-H. Lee, C. Broholm, N. P. Raju, and J. E. Greedan, Phys. Rev. Lett. **83**, 211 (1999).
[20] P. A. Lee, Science **321**, 1306 (2008).
[21] B. G. Levi, Physics Today **60**, 16 (2007).
[22] S. Nakatsuji, Y. Nambu, H. Tonomura, O. Sakai, S. Jonas, C. Broholm, H. Tsunetsugu, Y. Qiu, and Y. Maeno, Science **309**, 1697 (2005).
[23] P. Mendels, F. Bert, M. A. de Vries, A. Olariu, A. Harrison, F. Duc, J. C. Trombe, J. S. Lord, A. Amato, and C. Baines, Phys. Rev. Lett. **98**, 077204 (2007).
[24] V. Simonet, R. Ballou, J. Robert, B. Canals, F. Hippert, P. Bordet, P. Lejay, P. Fouquet, J. Ollivier, and D. Braithwaite, Phys. Rev. Lett. **100**, 237204 (2008).
[25] Y. Okamoto, M. Nohara, H. Aruga-Katori, and H. Takagi, Phys. Rev. Lett. **99**, 137207 (2007).
[26] J. S. Gardner, S. R. Dunsiger, B. D. Gaulin, M. J. P. Gingras, J. E. Greedan, R. F. Kiefl, M. D. Lumsden, W. A. MacFarlane, N. P. Raju, J. E. Sonier, et al., Phys. Rev. Lett. **82**, 1012 (1999).
[27] J. S. Gardner, B. D. Gaulin, A. J. Berlinsky, P. Waldron, S. R. Dunsiger, N. P. Raju, and J. D. Greedan, Phys. Rev. B **64**, 224416 (2001).
[28] J. S. Gardner, A. Keren, G. Ehlers, C. Stock, E. Segal, J. M. Roper, B. Fåk, M. B. Stone, P. R. Hammar, D. H. Reich, et al., Phys. Rev. B **68**, 180401(R) (2003).
[29] However, some studies have reported glassy behavior. See Refs. 50, 53 and 52.
[30] M. J. P. Gingras, B. C. den Hertog, M. Faucher, J. S. Gardner, S. R. Dunsiger, L. J. Chang, B. D. Gaulin, N. P. Raju, and J. E. Greedan, Phys. Rev. B. **62**, 6496 (2000).
[31] I. Mirebeau, A. Apetrei, I. N. Goncharenko, and R. Moessner, Physica **B385**, 307 (2006).
[32] M. Enjalran, M. J. P. Gingras, Y.-J. Kao, A. D. Maestro, and H. R. Molavian, J. Phys.: Condens Matter **16**, 5673 (2004).
[33] H. R. Molavian, M. J. P. Gingras, and B. Canals, Phys. Rev. Lett. **98**, 157204 (2007).
[34] A. L. Chernyshev, D. Galanakis, P. Phillips, A. V. Rozhkov, and A.-M. S. Tremblay, Phys. Rev. B **70**, 235111 (2004).
[35] J.-Y. P. Delannoy, M. J. P. Gingras, P. C. W. Holdsworth, and A.-M. S. Tremblay, Phys. Rev. B **72**, 115114 (2005).
[36] J.-Y. P. Delannoy, M. J. P. Gingras, P. C. W. Holdsworth, and A.-M. S. Tremblay, Phys. Rev. B **79**, 235130 (2009).
[37] R. G. Leigh, P. Phillips, and T.-P. Choy, Phys. Rev. Lett. **99**, 046404 (2006).
[38] M. Hermele, M. P. A. Fisher, and L. Balents, Phys. Rev. B **69**, 064404 (2004).
[39] A. H. C. Neto, P. Pujol, and E. Fradkin, Phys. Rev. B **74**, 024302 (2006).

[40] E. A. Goremychkin, R. Osborn, B. D. Rainford, R. T. Macaluso, D. T. Adroja, and M. Koza, Nature Physics **4**, 766 (2008).

[41] R. G. Melko, B. C. den Hertog, and M. J. P. Gingras, Phys. Rev. Lett. **87**, 067203 (2001).

[42] S. Rosenkranz, A. P. Ramirez, A. Hayashi, R. J. Cava, R. Siddharthan, and B. S. Shastry, J. Appl. Phys. **87**, 5914 (2000).

[43] I. Mirebeau, P. Bonville, and M. Hennion, Phys. Rev. B **76**, 184436 (2007).

[44] $\langle V \rangle$ denotes symbolically the energy scale of the interactions V, defined as the maximum of the exchange coupling and the dipole-dipole coupling.

[45] B. C. den Hertog and M. J. P. Gingras, Phys. Rev. Lett. **84**, 3430 (2000).

[46] S. T. Bramwell, M. J. Harris, B. C. den Hertog, M. J. P. Gingras, J. S. Gardner, D. F. McMorrow, A. R. Wildes, A. L. Cornelius, J. D. M. Champion, R. G. Melko, et al., Phys. Rev. Lett. **87**, 047205 (2001).

[47] T. Yavors'kii, T. Fennell, M. J. P. Gingras, and S. T. Bramwell, Phys. Rev. Lett. **101**, 037204 (2008).

[48] R. G. Melko and M. J. P. Gingras, J. Phys.:Condens. Matter **16**, R1277 (2004).

[49] A. P. Ramirez, A. Hayashi, R. J. Cava, R. Siddharthan, and B. S. Shastry, Nature **399**, 333 (1999).

[50] N. Hamaguchi, T. Matsushita, N. Wada, Y. Yasui, and M. Sato, Phys. Rev. B. **69**, 132413 (2004).

[51] X. Ke, D. V. West, R. J. Cava, and P. Schiffer, Phys. Rev. B **80**, 144426 (2009).

[52] G. Luo, S. T. Hess, and L. R. Corruccini, Phys. Lett. A. **291**, 306 (2001).

[53] Y. Yasui, M. Kanada, M. Ito, H. Harashina, M. Sato, H. Okumura, K. Kakura, and H. Kadawski, J. Phys. Soc. Jpn. **71**, 599 (2002).

[54] M. Enjalran and M. J. P. Gingras, Phys. Rev. B. **70**, 174426 (2004).

[55] Y.-J. Kao, M. Enjalran, A. D. Maestro, H. R. Molavian, and M. J. P. Gingras, Phys. Rev. B. **68**, 172407 (2003).

[56] J. Oitmaa, C. Hamer, and W. Zheng, Series Expansion Methods For Strongly Interacting Lattice Models (Cambridge University Press, 2006).

[57] M. J. Hutchings, Solid State Phys. **16**, 227 (1964).

[58] K. W. H. Stevens, Proc. Phys. Soc., London **A65**, 209 (1952).

[59] A. J. Freeman and J. P. Desclaux, J. Mag. and Mag. Mat. **12**, 11 (1979).

[60] This relation is consistent with the sign change of angular momentum operators under time reversal operation $\mathfrak{T}$ associated with antiunitary operator θ - the anticommutation of J and θ. For then $J^z(\theta|J,M\rangle) = -M(\theta|J,M\rangle)$ and $J^{\pm}(\theta|J,M\rangle) = \theta J^{\mp}|J,M\rangle = -\sqrt{(J\mp M+1)(J\pm 1)}(\theta|J,M\mp 1\rangle)$ from which one has the relation $\theta|J,M\rangle = (-)^{J-M}|J,M\rangle$. This ensures that a wavefunction is invariant under time reversal provided $c^M = (-)^{J-M}c^{-M}$.

[61] Ref. 43 estimates the exchange by fitting the experimental Curie-Weiss temperature to a model with crystal field and an isotropic exchange coupling that is treated within mean field theory.

[62] In retaining $V = H_{\rm ex} + H_{\rm dd}$ in Eq. (5) as our microscopic model of $Tb_2Ti_2O_7$, we were guided by the observation that this model does a good job in describing the inelastic and diffuse neutron scattering of $Tb_2Ti_2O_7$ in the paramagnetic regime (Ref.[55]).

[63] P. A. McClarty, S. H. Curnoe, and M. J. P. Gingras, J. Phys.: Conference Series **145**, 012032 (2009).

[64] P. Santini, S. Carretta, G. Amoretti, R. Caciuffo, N. Magnani, and G. H. Lander, Rev. Mod. Phys. **81**, 807 (2009).

[65] I. Lindgren and J. Morrison, Atomic Many-Body Theory (Springer-Verlag, 1982).

[66] D. L. Bergman, R. Shindou, G. A. Fiete, and L. Balents, Phys. Rev. B **75**, 094403 (2007).

[67] H. R. Molavian and M. J. P. Gingras, J. Phys.: Condens. Matter **21**, 172201 (2009).

[68] T. Fennell, O. A. Petrenko, B. Fak, S. T. Bramwell, M. Enjalran, T. Yavors'kii, M. J. P. Gingras, R. G. Melko, and G. Balakrishnan, Phys. Rev. B **70**, 134408 (2004).

[69] This zero temperature transition at $\mathcal{J}_{\rm ex}/\mathcal{D} = 4.525$ corresponds to the boundary at $J_{\rm nn}/D_{\rm nn} = -0.905$ in Ref. 41 since (i) here we have switched the sign convention for antiferromagnetic $\mathcal{J}_{\rm ex}$ compared to Ref. 41 and (ii) since we have $J_{\rm nn}$ and $D_{\rm nn}$ here given by $J_{\rm nn} = \mathcal{J}_{\rm ex}\langle\tilde{J}^z\rangle^2/3$ and $D_{\rm nn} = 5\mathcal{D}\langle\tilde{J}^z\rangle^2/3$.

[70] It is also because exchange couplings beyond nearest neighbors are weak in comparison to the Ising interactions such that there exists a prevailing (classical) Ising energy scale set by $\mathcal{PHP}$. See Refs. 47 and 68.

[71] The bare nearest neighbor isotropic exchange $\mathcal{J}_{\rm ex}$ is not known with good precision. There are currently differing estimates of $\mathcal{J}_{\rm ex}$ in the literature.[30,43] Also, further neighbor exchange is measurable, at least in the spin ice $Dy_2Ti_2O_7$,[47] (see also Ref. 98) so it is not unlikely that further neighbor interactions also play a role in the physics of other rare earth titanates including $Tb_2Ti_2O_7$.

[72] A. S. Wills, M. E. Zhitomirsky, B. Canals, J. P. Sanchez, P. Bonville, P. D. de Réotier, and A. Yaouanc, J. Phys.: Condens. Matter **18**, L37 (2006).

[73] A. D. Maestro and M. J. P. Gingras, Phys. Rev. B **76**, 064418 (2007).

[74] A. Keren, J. S. Gardner, G. Ehlers, A. Fukaya, E. Segal, and Y. J. Uemura, Phys. Rev. Lett. **92**, 107204 (2004).

[75] J. van Duijn, K. H. Kim, N. Hur, D. Adroja, M. A. Adams, Q. Z. Huang, M. Jaime, S.-W. Cheong, C. Broholm, and T. G. Perring, Phys. Rev. Lett. **94**, 177201 (2005).

[76] S. W. de Leeuw, J. W. Perram, and E. R. Smith, Proc. Roy. Soc. London **373**, 27 (1980).

[77] H. R. Molavian, Ph. D. thesis, U. of Waterloo (2007).

[78] Admixing between the excited crystal field states is neglected in this model, (a consequence of studying the effective Hamiltonian to second order in perturbation theory and neglecting higher order terms), which should be a good approximation because the splitting between the first excited doublet and the next excited singlet is about 120 K. Note that in the remainder of the article all excited crystal field states are included in our derivation of $H_{\rm eff}$.

[79] A. Poole, A. S. Wills, and E. Lelièvre-Berna, J. Phys.:Condens. Matter **19**, 452201 (2007).

[80] It is worth noting here that since the ordering of the XY components is the same ordering found in $Er_2Ti_2O_7$ which has an almost perfect XY anisotropy. Given that the ordering mechanism $Er_2Ti_2O_7$ is currently not understood,[63] this result might lead one to suspect that three spin interactions produced by VCFEs are responsible. This turns out not to be the case: if one computes the effective Hamiltonian for $Er_2Ti_2O_7$, one finds that the time reversal properties of the effective spins are the same as for ordinary

angular momenta (in contrast to $Tb_2Ti_2O_7$ effective spins) so that effective three spin interactions cannot appear in this case.

[81] I. Mirebeau, A. Apetrei, J. Rodrguez-Carvajal, P. Bonville, A. Forget, D. Colson, V. Glazkov, J. P. Sanchez, O. Isnard, and E. Suard, Phys. Rev. Lett. **94**, 246402 (2005).

[82] Note that the ground to first excited crystal field gap in spin ice $Ho_2Ti_2O_7$ is about 250 K, which might suggest that VCFEs could be significant based on the fact that the $LRSI_{000}$ phase appears at about this value of Δ. However, $\mathcal{J}_{ex}/\mathcal{D}$ in $Ho_2Ti_2O_7$ places this material in the $LRSI_{001}$ part of the phase diagram as one would expect from the DSIM.

[83] K. C. Rule, J. P. C. Ruff, B. D. Gaulin, S. R. Dunsiger, J. S. Gardner, J. P. Clancy, M. J. Lewis, H. A. Dabkowska, I. Mirebeau, P. Manuel, et al., Phys. Rev. Lett. **96**, 177201 (2006).

[84] I. Mirebeau, I. N. Goncharenko, P. Cadavez-Peres, S. T. Bramwell, M. J. P. Gingras, and J. S. Gardner, Nature **420**, 54 (2002).

[85] T. T. A. Lummen, I. P. Handayani, M. C. Donker, D. Fausti, G. Dhalenne, P. Berthet, A. Revcolevschi, and P. H. M. van Loosdrecht, Phys. Rev. B. **78**, 094418 (2008).

[86] J. P. C. Ruff, B. D. Gaulin, J. P. Castellan, K. C. Rule, J. P. Clancy, and J. Rodriguez, Phys. Rev. Lett. **99**, 237202 (2007).

[87] J. D. Thompson, P. A. McClarty, H. M. Rønnow, L. P. Regnault, A. Sorge, and M. J. P. Gingras, (unpublished).

[88] H. D. Zhou, C. R. Wiebe, J. A. Janik, L. Balicas, Y. J. Yo, Y. Qiu, J. R. D. Copley, and J. S. Gardner, Phys. Rev. Lett. **101**, 227204 (2008).

[89] S. Nakatsuji, Y. Machida, Y. Maeno, T. Tayama, T. Sakakibara, J. van Duijn, L. Balicas, J. N. Millican, R. T. Macaluso, and J. Y. Chan, Phys. Rev. Lett. **96**, 087204 (2009).

[90] K. Matsuhira, C. Sekine, C. Paulsen, M. Wakeshima, Y. Hinatsu, T. Kitazawa, Y. Kiuchi, Z. Hiroi, and S. Takagi, J. Phys.: Conference Series **145**, 012031 (2009).

[91] J. Robert, V. Simonet, B. Canals, R. Ballou, P. Bordet, P. Lejay, and A. Stunault, Phys. Rev. Lett. **96**, 197205 (2006).

[92] P. Bordet, I. Gelard, K. Marty, A. Ibanez, J. Robert, V. Simonet, B. Canals, R. Ballou, and P. Lejay, J. Phys.: Condens. Matter **18**, 5147 (2006).

[93] H. D. Zhou, B. W. Vogt, J. A. Janik, Y.-J. Jo, L. Balicas, Y. Qiu, J. R. D. Copley, J. S. Gardner, and C. R. Wiebe, Phys. Rev. Lett. **99**, 236401 (2007).

[94] L. L. Lumata, K. Y. Choi, T. Besara, M. J. R. Hoch, H. D. Zhou, J. S. Brooks, P. L. Kuhns, A. P. Reyes, N. S. Dalal, and C. R. Wiebe, arXiv:0811.3367.

[95] H. D. Zhou, C. R. Wiebe, L. Balicas, Y.-J. Jo, Y. Takano, M. J. Case, Y. Qiu, J. R. D. Copley, and J. S. Gardner, Phys. Rev. Lett. **102**, 067203 (2009).

[96] A. Kassman, J. Chem. Phys. **53**, 4118 (1970).

[97] J. Jensen and A. Mackintosh, Rare Earth Magnetism (Oxford University Press, 1991).

[98] J. P. C. Ruff, R. G. Melko, and M. J. P. Gingras, Phys. Rev. Lett. **95**, 097202 (2005).